POLYTECHNIQUE MONTRÉAL
affiliée à l'Université de Montréal

Exploiting Geometric Frustration in Coupled von Mises Trusses to Program Multifunctional Mechanical Metamaterials

YANNIS JOSEPH BERNARD LIÉTARD
Département de génie mécanique

Mémoire présenté en vue de l'obtention du diplôme de *Maîtrise ès sciences appliquées*
Génie aérospatial

Septembre 2024

POLYTECHNIQUE MONTRÉAL
affiliée à l'Université de Montréal

Ce mémoire intitulé :

Exploiting Geometric Frustration in Coupled von Mises Trusses to Program Multifunctional Mechanical Metamaterials

présenté par **Yannis Joseph Bernard LIÉTARD**
en vue de l'obtention du diplôme de *Maîtrise ès sciences appliquées*
a été dûment accepté par le jury d'examen constitué de :

Sampada BODKHE, présidente
David MÉLANÇON, membre et directeur de recherche
Daniel THERRIAULT, membre et codirecteur de recherche
Damiano PASINI, membre

ACKNOWLEDGEMENTS

I would like to express my warmest appreciation to my supervisors, David Mélançon and Daniel Therriault, for giving me the opportunity to work on this project and for their guidance throughout this journey. Their trust in my abilities encouraged creativity in my work, and their continuous support helped me overcome numerous challenges. Beyond the professional sphere, I also fondly remember the many moments we shared outside of work, which made this experience all the more enriching and helped me feel fully integrated into the team. Their mentorship has had a lasting impact on my development as a researcher and strengthened my confidence in pursuing future opportunities.

I extend my gratitude to all the technicians who provided me helpful assistance during my experimental tests and with the 3D printers: Kambiz Chizari, Yanik Landry-Ducharme, and Christian Charles Martel. I am deeply grateful to Danick Lamoureux, Josua Garon, Juliette Pierre, Luca Boisneault, Mathieu Verville, Negar Aghigh, Olivier Duchesne, Richard Marcotte, and Saeideh Kazembeigi, who generously shared their knowledge, trained me on lab equipment, assisted with my simulations and models, and whose invaluable conversations provided insights that greatly supported my progress. A special thank you goes to Nina Tricot, whose help in fabricating and testing prototypes was indispensable. It was a true pleasure working with you.

I will never forget the members of LM2. Your friendship made me feel at home, even though I was far from my country. LM2 is truly a Phamille, and I am lucky to have been a part of such a welcoming and supportive group.

I would also like to acknowledge the financial support of the Natural Sciences and Engineering Research Council of Canada.

Lastly, this experience abroad would not have been as fulfilling without the unwavering support of my family. To my parents and my sister, thank you for always encouraging me, believing in me, and even visiting me during this journey. Your love and support kept me going through the challenges. I also want to thank my friends back in France—Arthur, Camille, Elise, Hugo, Lauranne, and Philippine. Your friendship has been a constant source of strength throughout this experience.

RÉSUMÉ

Les métamatériaux mécaniques multistables constituent une classe émergente de matériaux artificiels dont les propriétés mécaniques sont déterminées par leur structure interne plutôt que par la composition de leurs matériaux de base. Ces matériaux sont capables de passer d'un état d'énergie stable à un autre. Motivé par le besoin de créer des métamatériaux plus polyvalents et multifonctionnels—c'est-à-dire capables d'accomplir plusieurs fonctions différentes au sein d'une même structure—ce travail vise à développer un métamatériau mécanique multistable combinant trois propriétés : une rigidité effective variable, la capacité à changer de forme et la modularité post-fabrication. Le point de départ est un bloc de construction consistant en un assemblage de barreaux de von Mises bistables. Tout d'abord, nous montrons que le couplage de deux de ces structures bistables induit de la frustration géométrique, et ainsi, une asymétrie entre les deux états stables. Nous combinons ensuite ces blocs pour construire une unité capable de modifier sa rigidité effective en compression et sa hauteur lors du passage d'un état stable à l'autre.

Des simulations par éléments finis sont utilisées pour étudier trois géométries distinctes, chacune correspondant à l'un des scénarios suivants : (1) augmentation, (2) diminution ou (3) rigidité en compression et hauteur constantes entre les deux états stables. Pour valider le concept, nous fabriquons nos métamatériaux multistables en acide polylactique (PLA) et en polyuréthane thermoplastique (TPU) via la fabrication par filament fondu (FFF) et évaluons leur réponse mécanique en mesurant expérimentalement, dans les deux états stables, leur rigidité effective en compression. Nous explorons l'espace de design en développant un modèle semi-analytique nous permettant d'approfondir notre compréhension des mécanismes sous-jacents à l'origine de la variation de rigidité et de hauteur.

Après une validation théorique et expérimentale, nous étudions plusieurs applications de l'unité. Nous commençons par démontrer la capacité à reprogrammer la variation de la rigidité post-fabrication grâce à son design modulaire. Nous construisons ensuite un panneau sandwich dont la rigidité en compression et en flexion est variable. Enfin, nous exploitons la capacité des unités à changer de forme pour créer un panneau sandwich avec une surface dont la courbure peut être modifiée. Les résultats obtenus font l'objet d'un article soumis à Advanced Engineering Materials pour un numéro spécial intitulé "Additive Manufacturing-Enabled Cellular Materials". Nous pensons que la polyvalence et la multifonctionnalité du métamatériau proposé offrent un potentiel important pour les applications d'ingénierie moderne, où les fonctionnalités avancées sont cruciales, telles que l'aérospatiale, l'automobile et le secteur biomédical.

ABSTRACT

Multistable mechanical metamaterials are an emerging class of engineered materials whose mechanical properties are determined by their structural design rather than by the composition of the base materials. These materials are capable of switching from one stable energy state to another. Motivated by the need to create more versatile and multifunctional metamaterials-i.e., capable of performing several different functions within the same structure-this work presents the development of a multistable mechanical metamaterial combining three properties : stiffness tunability, shape morphing and modularity. The proposed design is based on a bottom-up strategy, whose starting point is a building block consisting in an assembly of bistable von Mises trusses. First, we show that coupling two von Mises trusses induces geometric frustration, a phenomenon where the system cannot simultaneously satisfy all structural constraints, which leads to an inherent asymmetry between the two stable states. We then combine the building blocks to build a unit cell that can change effective stiffness in compression and height when switching from one stable state to the other.

Finite element simulations are utilized to study three distinct geometries, each corresponding to one of the following scenarios: (1) increased; (2) decreased or (3) constant stiffness and height between the stable states. To validate the concept, we fabricate our multistable metamaterials out of polylactic acid (PLA) and thermoplastic polyurethane (TPU) via fused filament fabrication (FFF) and evaluate their mechanical response by measuring experimentally the effective stiffness in both stable states under compression. We further explore the design space by developing a semi-analytical model, allowing us to deepen our understanding of the underlying mechanisms driving stiffness and shape variation.

In addition to theoretical and experimental validation, we investigate several applications of the developed unit cell. We start by demonstrating the ability to reprogram the stiffness variation post-fabrication through modularity. Subsequently, we build a sandwich panel whose rigidity in compression and bending can be tuned. Finally, we leverage the shape morphing capabilities of the unit cells to create a sandwich panel with a morphing surface. The full results of this work have been submitted to Advanced Engineering Materials for a special issue titled "Additive Manufacturing-Enabled Cellular Materials". We believe that the versatility and the multifunctionality of the proposed metamaterial hold significant potential for advanced engineering applications, where enhanced functionalities are crucial, such as aerospace, automotive and biomedical sectors.

TABLE OF CONTENTS

LIST OF FIGURES

LIST OF SYMBOLS AND ACRONYMS

Acronyms

2D	Two-dimensional
3D	Three-dimensional
EPDM	Ethylene Propylene Diene Monomer
FFF	Fused Filament Fabrication
FE	Finite Element
LM2	Laboratory for Multi-scale Mechanics
NSERC	National Science and Engineering Research Council
PLA	PolyLactic Acid
TPU	Thermoplastic PolyUrethane
UV	UltraViolet

Symbols

$(\cdot)_{exp}$	Used to refer to experimental results
E_0	Initial Young's modulus
$(\cdot)_{FE}$	Used to refer to finite element simulation results
$(\cdot)^{iso}$	Used to refer to the isostiffness unit
K_{min}	Minimum theoretical stiffness
K_{max}	Maximum theoretical stiffness
K_{0000}	Stiffness of a unit in state 0000
K_{1111}	Stiffness of a unit in state 1111
L	Initial length of a truss in von Mises truss
L_{0xy}	Initial length of the von Mises truss in the xy-plane
L_{0xz}	Initial length of the von Mises truss in the xz-plane
r_L	Ratio of the initial lengths of the coupled von Mises truss ($r_L = L_{0xy}/L_{0xz}$)
$(\cdot)_{sa}$	Used to refer to semi-analytical results
$(\cdot)^{sandwich}$	Used to refer to the 3×2 sandwich panel
$(\cdot)^{soft}$	Used to refer to the softening unit
$(\cdot)^{stiff}$	Used to refer to the stiffening unit
α	First unit geometry for the sandwich panel with a morphing surface

β	Second unit geometry for the sandwich panel with a morphing surface
δ	Displacement applied at the apex of a von Mises truss
Δ	Algebraic distance in a coupled von Mises truss between the first line connecting the two ends of the von Mises truss in the xz-plane and the second line connecting the ends of the von Mises truss in the xy-plane
η	Stiffness variation ($\eta = K_{1111}/K_{0000}$)
η'	Stiffness variation after replacing the von Mises trusses by a new geometry
θ	Initial angle of inclination of a truss in a von Mises truss
θ_{0xy}	Initial angle of the von Mises truss in the xy-plane
θ_{0xz}	Initial angle of the von Mises truss in the xz-plane
κ_x	Curvature of the surface along the x-axis
κ_y	Curvature of the surface along the y-axis

CHAPTER 1 INTRODUCTION

Modern engineering systems require increasingly sophisticated functionalities surpassing the capabilities of conventional materials. Structural components in the aerospace and automotive sectors must be lightweight yet support important loading. Materials used in space must withstand harsh environments and medical implants must be both tailored to the patient and biocompatible. Although natural materials are fundamental, they offer only a restricted range of mechanical properties that may not fully meet the requirements of future applications. To overcome these inherent limitations, recent research has been focusing on mechanical metamaterials—materials whose mechanical properties are governed by their structure rather than the composition of their base materials. These metamaterials are designed to achieve mechanical properties and functionalities that are not typically found in nature. Advances in three-dimensional (3D) printing techniques played a major role in this progress, enabling the fabrication of complex structures with a wide range of materials. However, the field of mechanical metamaterials still faces challenges, particularly in achieving multiple tunable properties within a single metamaterial design.

Indeed, in soft robotics, the stiffness of a metamaterial can be tuned to allow a soft gripper to handle objects with varying shapes and rigidity (Zhai et al., 2020). In aerospace, metamaterials with shape morphing abilities can lead to aerodynamic structures capable of controlling their drag (Terwagne et al., 2014). Modularity is leveraged to reprogram the snapping behavior of a multistable metamaterial (Mao et al., 2022). Yet, these properties have mostly been developed independently. Integrating multiple tunable properties within a single metamaterial could lead to enhanced multifunctionality for cutting-edge engineering applications. This work aims at designing and 3D printing a versatile multistable mechanical metamaterial that combines tunable stiffness, shape morphing, and modularity. A bottom-up strategy in three steps is adopted. We start with a building block composed of coupled von Mises trusses. Next, we combine several building block to form a unit cell with tunable properties. Finally, various applications are explored, including a sandwich panel with adjustable compressive and bending stiffness, as well as one with a morphing surface.

The thesis is organized as follows. Chapter 2 presents a brief literature review on mechanical metamaterials, focusing on multistability, stiffness tunability, shape morphing, and modularity, as well as fabrication methods through additive manufacturing. Chapter 3 synthesizes

the literature review and introduces the objectives of the thesis. Chapter 4 includes the article titled "Exploiting geometric frustration in coupled von Mises trusses to program multifunctional mechanical metamaterials", detailing the design, fabrication, and modeling of the proposed metamaterial, along with different applications. The supplementary information of this article is appended at the end of chapter 4. Finally, the conclusion and outlook discuss the results obtained and provide suggestions for improvements.

CHAPTER 2 LITERATURE REVIEW

2.1 Tailoring material properties through mechanical metamaterials

Metamaterials are architected materials designed to achieve unique properties. While the properties of conventional materials are primarily determined by their composition, those of metamaterials are mainly governed by their structural design. Mechanical metamaterials, in particular, aim to achieve exotic mechanical properties that they are not typically found in nature, such as ultra-low effective density (Schaedler et al., 2011), negative Poisson's ratio (J. T. B. Overvelde et al., 2012), negative thermal expansion (Q. Wang et al., 2016) or sequential snap-through behavior (Rafsanjani et al., 2015). Additionally, these materials can have tunable properties, such as tunable stiffness (Zhai et al., 2018) and shape morphing capabilities (Haghpanah et al., 2016). Metamaterials are typically composed of tessellations of unit cells, ranging in size from the nanoscale (Vyatskikh et al., 2018) to the macroscale (J. T. Overvelde et al., 2016). Figure 2.1 provides a visual overview of several levels of functionality achieved with regular materials and mechanical metamaterials across different scales.

2.2 Additive manufacturing of mechanical metamaterials

The development of metamaterials have been greatly facilitated by the advances in additive manufacturing, enabling the manufacture of complex intricate structures that would otherwise be complicated or impossible to fabricate by traditional means. These technologies, based on layer-by-layer fabrication process, make it possible to print unit cells at various scales with a large range of available materials. Some of the main techniques are presented bellow with examples of applications from the literature :

- **Vat photopolymerization.** Techniques using photopolymerization to create 3D parts by selectively curing a photosensitive liquid resin. They offer a very high manufacturing resolution (up to 10 µm) but the choice of materials is limited to photopolymers. Ultralight and ultrastiff mechanical metamaterials have been 3D printed at the microscale using projection microstereolithography (Zheng et al., 2014), where two-dimensional (2D) images corresponding to slices of the 3D model are used to cure a resin with ultraviolet (UV) (see Figure 2.2A).
- **Powder bed fusion.** Powder bed fusion techniques rely on a laser or an electron beam which selectively fuses a powder layer by layer to print metallic or polymeric

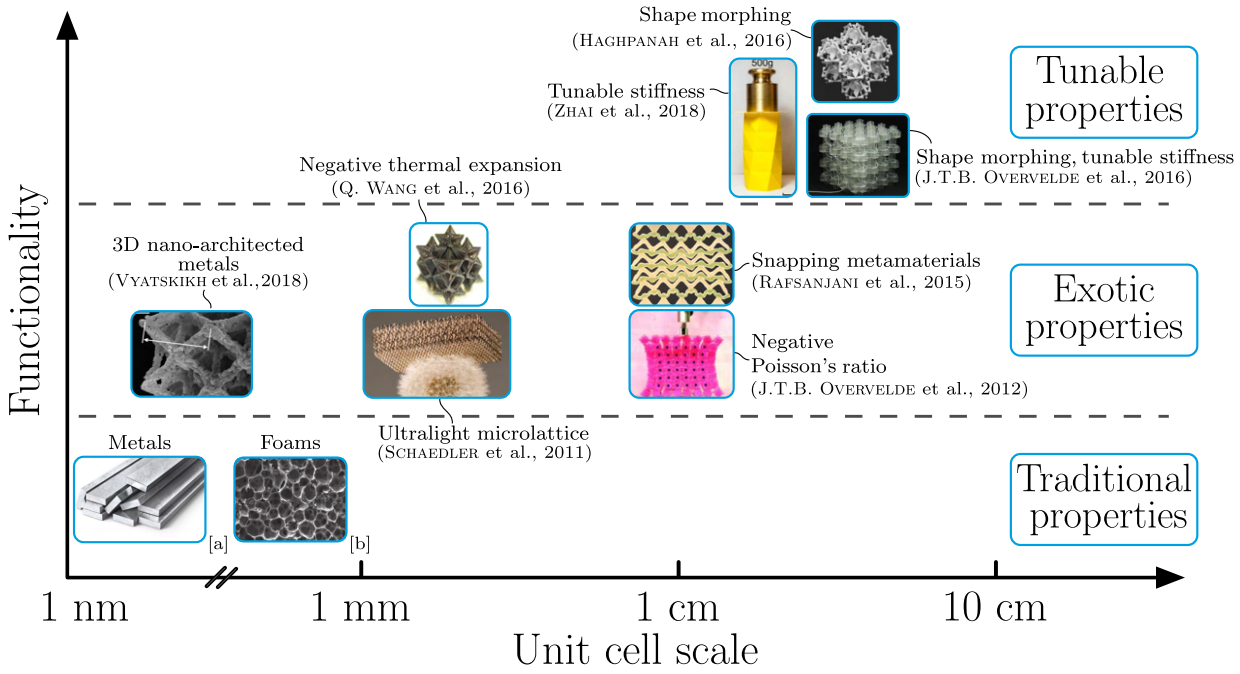

Figure 2.1 | **Tailoring material properties through mechanical metamaterials** Traditional materials (e.g. metals or foam) exhibit limited mechanical properties. By rationally designing unit cells, mechanical metamaterials achieve unique functionalities that can not be found in nature. ([a] www.rocheindustry.com/types-of-metal/, [b] (Tondi et al., 2008))

materials. One of its advantages is that almost no support is required as the powder bed direclty acts as a support, making it particularly useful for fabricating complex lattice structures such as 3D multistable shellular metamaterials (Shi et al., 2021). A disadvantage of this method is that it is inherently monomaterial.

- **Material jetting.** In material jetting, droplets of UV-curable material are sprayed on a printing bed to build a part layer by layer. The main advantage of this technique lies in its ability to print multi-material parts with good accuracy (up to 10 µm), but it is limited to photopolymers. H. Zhang et al., 2021 use this technique to build multistable mechanical metamaterials that can be used as ternary logic gates and amplitude modulator.

- **Material extrusion.** Extrusion techniques are divided in two categories. The first one is Direct Ink Writing (DIW) which is based on the extrusion of viscoelastic ink to form a solid part. Although the geometries that can be printed are limited, DIW can be used with a wide range of materials. Y. Jiang et al., 2019 use DIW to print anisotropic composite structure responsive to stimuli and programmed to actuate at a given time (see Figure 2.2B). The second technique based on material extrusion is Fused

Filament Fabrication (FFF). FFF is based on the extrusion of thermoplastic filaments with a heated nozzle. This method can be used with a wide range of materials but is limited by its low printing resolution (up to 50 µm). As shown in Figure 2.2C, FFF is particularly interesting for origami-inspired metamaterials because of its simplicity, affordability, and capability to print multimaterial parts. For instance, soft materials are required for the flexible joints, while stiff materials are necessary for the rigid panels (Q. Liu et al., 2023).

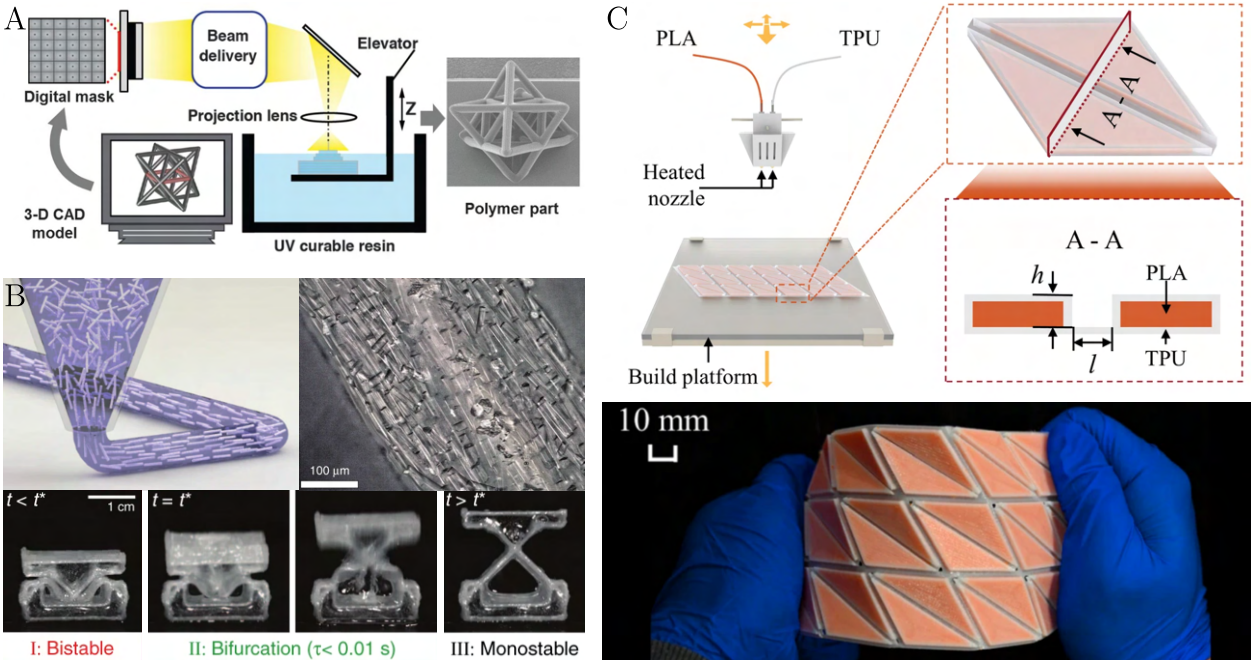

Figure 2.2 | **Additive manufacturing of mechanical metamaterials (A)** Ultralight and ultrastiff microlattices 3D printed using projection microstereolithography (reproduced from Zheng et al., 2014 with permission from the American Association for the Advancement of Science at `https://doi.org/10.1126/science.1252291`) **(B)** Fabrication of anisotropic composite structures responding to environmental stimuli to trigger self-actuation at a specific time using DIW (reproduced from Y. Jiang et al., 2019 with permission from Springer Nature due to its open-access status) **(C)** Origami inspired structures can be fabricated using FFF. Thermoplastic polyurethane (TPU) is used for the soft hinges and stiff panels are made of polylactic acid (PLA) (reproduced from Q. Liu et al., 2023 with permission from Springer Nature at `https://doi.org/10.1007/s10338-023-00403-1`).

2.3 Multistability for enhanced functionality

Although geometric non-linearities and elastic instabilities are avoided in traditional engineering structures, recent advances in flexible metamaterials have demonstrated that en-

abling large deformations can lead to novel functionalities such as multistability (Bertoldi et al., 2017). Multistable structure possess multiple minimum of energy corresponding to different stable states, unlike regular structures which typically have a single stable state. Multistability is achievable through many ways, which can be categorized in different types (Chi et al., 2022) : constrained 1D beams/trusses (Restrepo et al., 2015) (see Figure 2.3A), curved 2D plates (Forterre et al., 2005), 3D shells (Abbasi et al., 2024) (see Figure 2.3B), compliant mechanisms (Jensen et al., 1999), origami-inspired structures (Melancon et al., 2021) (see Figure 2.3C) and balloons (J. T. B. Overvelde et al., 2015). Multistability offers several advantages such as the ability to stay in a given configuration without needing continuous actuation and opens up new possibilities for tuning the properties of structures.

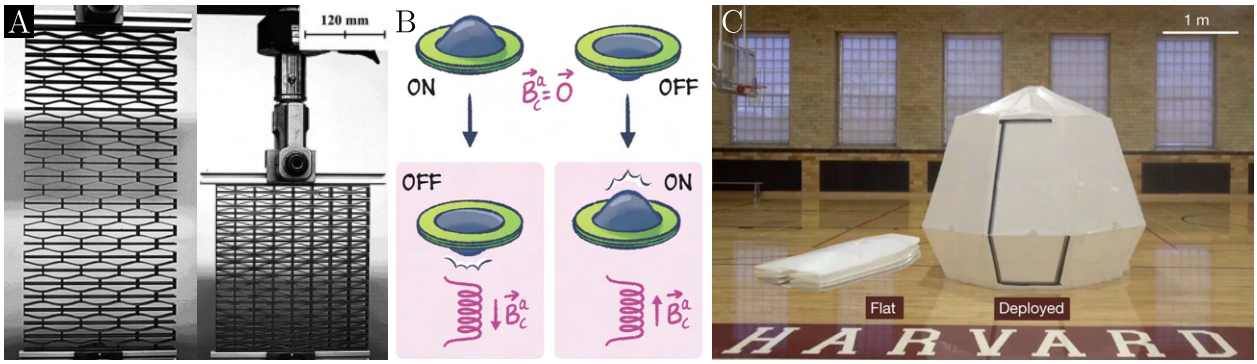

Figure 2.3 | **Multistability for enhanced functionality (A)** Multistable cellular material based on constrained beams (reproduced from Restrepo et al., 2015 with permission from Elsevier at `https://doi.org/10.1016/j.eml.2015.08.001`) **(B)** Programmable braille reader based on bistable shells (reproduced from Abbasi et al., 2024 with permission from John Wiley & Sons at `https://doi.org/10.1002/admt.202301344`) **(C)** Multistable inflatable origami inspired shelter in flat and deployed state (reproduced from Melancon et al., 2021 with permission from Springer Nature at `https://doi.org/10.1038/s41586-021-03407-4`)

2.4 Mechanical metamaterials with tunable stiffness

Among many applications, the concept of multistability has significantly enhanced the functionalities of metamaterials. A notable example is mechanical metamaterials with tunable stiffness, where different stable states can exhibit different stiffness values. Various strategies have been employed to achieve tunable stiffness, mainly focusing on tuning compressive stiffness. Origami appears as a very prolific platform, as several works have demonstrated the potential of well-known origami patterns. For instance, the popping of creases in the kresling pattern has been used to create a stiffer stable states (Zhai et al., 2018; Wo and Filipov, 2023; X. Wang et al., 2023) (see Figure 2.4A), and geometric frustration caused by defects

in a multistable Miura-ori pattern has been leveraged to increase stiffness (Silverberg et al., 2014) (see Figure 2.4B). Additionally, in situ manipulation of compressive stiffness has also been realized by controlling the curvature of creases in curved origami (Zhai et al., 2020), by introducing zero modes through topological transformations in Kagome lattice structure—a two-dimensional network characterized by a repeating pattern of triangles and hexagons−(L. Wu and Pasini, 2024) or using bistable shells to build magnetically actuated physical binary elements (Chen et al., 2021). Beyond compressive stiffness, other types of stiffness have also been explored. Multistable kirigami structures have been investigated for tunable stiffness in tension (Yang et al., 2018) (see Figure 2.4C), while bending stiffness has been tuned through topological transformation associated with zero-energy modes in multistable lattice framework (L. Wu and Pasini, 2023) (see Figure 2.4D). Furthermore, chiral metamaterial has been designed to program the shear stiffness (Tahidul Haque et al., 2024) and bistable domes has been used as a unit cell to tune torsional stiffness (Udani and Arrieta, 2021).

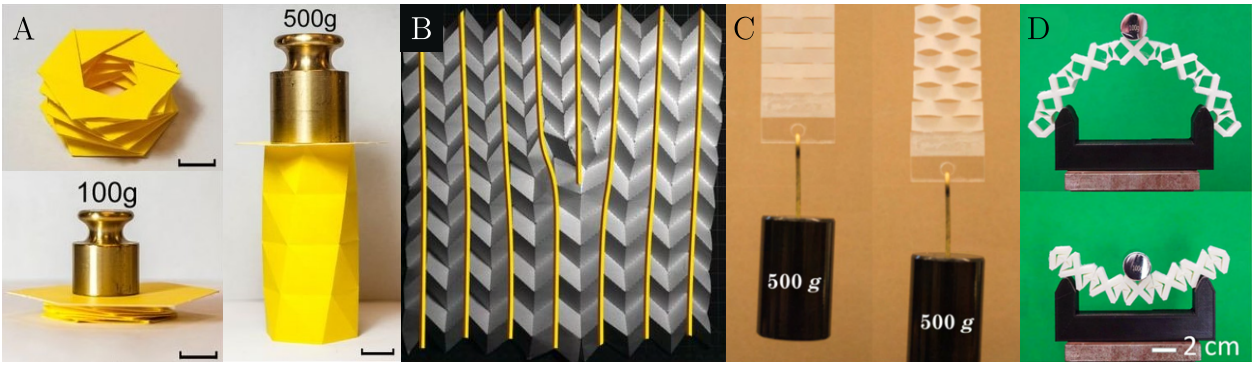

Figure 2.4 | **Mechanical metamaterials with tunable stiffness A.** The different stables states of a Kresling demonstrate distinct stiffness in compression (reproduced from Zhai et al., 2018 with permission from the National Academy of Sciences (U.S.) due to its open-access status). **B.** Pop-through defects in a multistable Miura-ori tesselation leads to an increase in compressive stiffness (reproduced from Silverberg et al., 2014 with permission from the American Association for the Advancement of Science at `https://doi.org/10.1126/science.1252876`). **C.** Multistable kirigami displays tunable stiffness in tension (reproduced from Yang et al., 2018 with permission from the American Physical Society at `https://doi.org/10.1103/PhysRevMaterials.2.110601`). **D.** Through topological transformations, a multistable lattice framework exhibit tunable bending stiffness (reproduced from L. Wu and Pasini, 2023 with permission from the American Physical Society at `https://doi.org/10.1103/PhysRevApplied.19.L061001`).

Stiffness tunability can be applied in various fields of research or industry. In soft robotics, tuning the gripping force of soft grippers makes robots safer for human interaction, more adaptive to handle objects with various shapes and fragility (Zhai et al., 2020; Tang et al., 2020). Tunable stiffness also proves to be useful for smart fabrics, with promising applications

in medical supports and exoskeletons (Y. Wang et al., 2021) It can also benefit drones, allowing them to avoid damage during collisions by softening, or fish-like robots capable of swimming efficiently by adapting the stiffness of their tails to their swimming speed (Zhong et al., 2021).

2.5 Shape morphing for adaptative structures

Another property attracting a lot of attention in recent research and industrial applications, particularly in the aerospace and automotive sectors, is shape morphing. Shape morphing refers to the ability of undergoing programmed and reversible deformations in response to external stimuli. Using a combinatorial design approach, patterned textures can be programmed in aperiodic metamaterials (Coulais et al., 2016) (see Figure 2.5A). Multistable mechanisms have been used to transform flat surfaces into curved ones, utilizing structures inspired by the von Mises truss (Chen and Shea, 2021) (see Figure 2.5B), topological transformations in lattice frameworks (L. Wu and Pasini, 2023), kirigami (C. Jiang et al., 2022), corrugated sheets (Meeussen and Van Hecke, 2023) (see Figure 2.5C) and two-way shape memory polymer effect (Risso et al., 2024). Shape morphing can also be extended to three-dimensional structures (Haghpanah et al., 2016; J. T. Overvelde et al., 2016). Different actuation methods can be used such as materials sensitive to temperature (Y. Wu et al., 2023; Hwang et al., 2022; Risso et al., 2024), hydrophilic materials (Raviv et al., 2014) (see Figure 2.5D) and pneumatic actuation (J. T. Overvelde et al., 2016; Terwagne et al., 2014; Siéfert et al., 2019) (see Figure 2.5E).

Shape morphing leads to innovative applications in various fields. For instance, controlling the texture of a surface allows for the adjustment of aerodynamic drag, which can be useful in aerodynamic structure (Terwagne et al., 2014). Soft robotic drones can change configuration to transform into a ground vehicule, offering versatile mobility (Hwang et al., 2022). In the biomedical sector, deployable implants, capable of expanding after insertion in the human body, can be used for minimally invasive surgery (Bobbert et al., 2020).

2.6 Reprogramming and reconfiguration through modularity

Finally, modularity has been recently introduced in the design of metamaterials. A modular approach involves systems consisting of smaller individual components that can be separated and recombined, similar to LEGO bricks. It has proven to be a useful property to reprogram post-fabrication the snap-through behaviour of architected materials based on constrained beams (Mao et al., 2022) (see Figure 2.6A). Modularity has also been introduced in origami

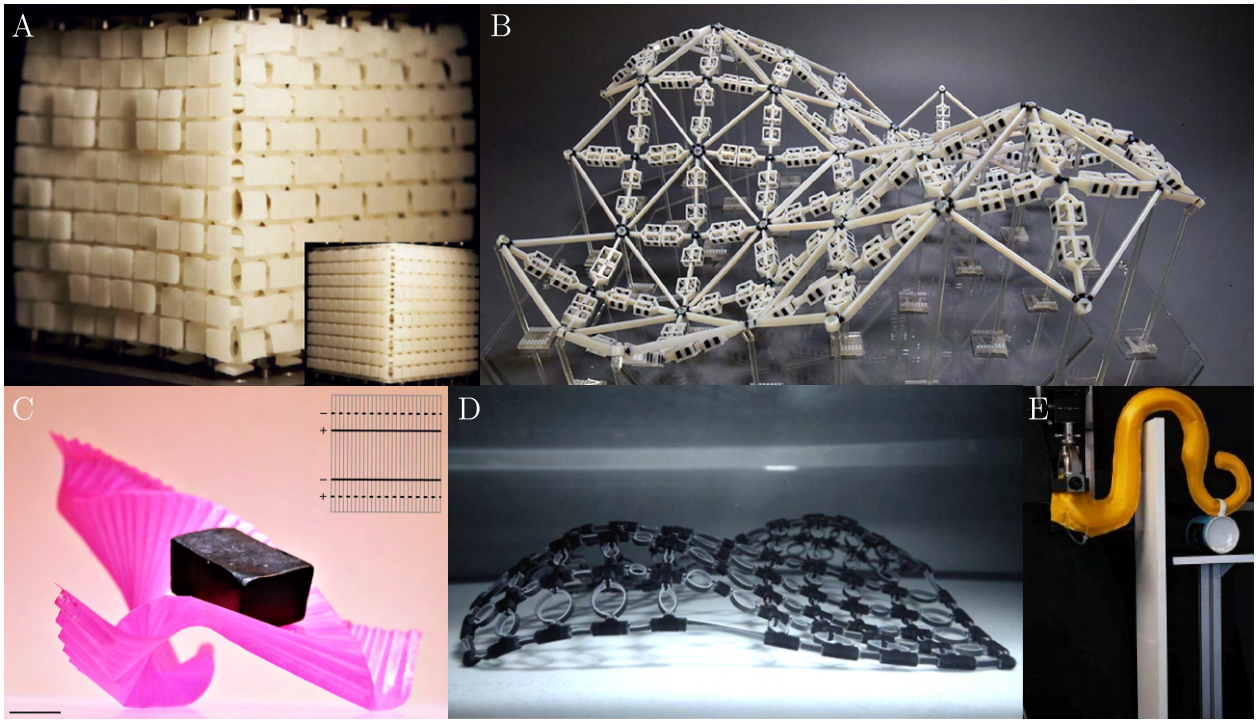

Figure 2.5 | **Shape morphing for adaptative structures (A)** Through a combinatorial method, a metacube is designed to display programmed texture when uniaxially compressed (reproduced from Coulais et al., 2016 with permission from Springer Nature at `https://doi.org/10.1038/nature18960`). **(B)** A planar surface made of combined bistable actuators is used to reconfigure into target shapes (reproduced from Chen and Shea, 2021 with permission from Elsevier due to its open-access status). **(C)** Undulating metasheets exhibit multistability and can be deformed reversibly by creating persisting scars (reproduced from Meeussen and Van Hecke, 2023 with permission from Springer Nature at `https://doi.org/10.1038/s41586-023-06353-5`). Scale bar, 2cm **D.** Multimaterial 3D printing enables the fabrication of a self-evolving structure capable of dynamically changing shape in response to environmental conditions, here water (reproduced from Raviv et al., 2014 with permission from Springer Nature due to its open-access status). **E.** The deformation of flat inflatable structures can be programmed to achieve specified curvilinear shapes (reproduced from Siéfert et al., 2019 with permission from the National Academy of Sciences (U.S.) at `https://doi.org/10.1073/pnas.1904544116`).

(Mousanezhad et al., 2017; Li et al., 2024; Zhu and Filipov, 2024) (see Figure 2.6B,C) and kirigami (Li et al., 2021) to make the assembly and the disassembly of modules easier, thereby expanding the range of possible reconfigurations and making the metamaterials more versatile.

Modularity can enhance the mechanical metamaterials functionality by enabling reprogramming of mechanical properties after fabrication and increasing the number of possible con-

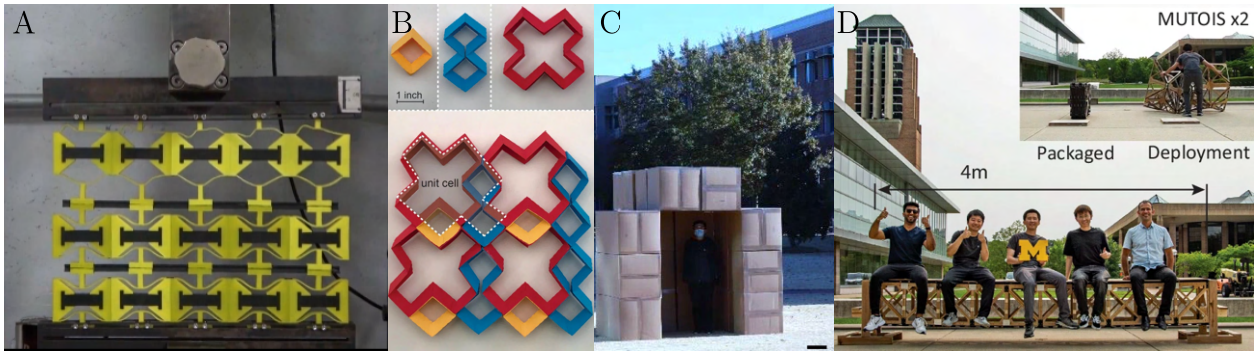

Figure 2.6 | **Reprogramming and reconfiguration through modularity (A)** The snap-through behavior of a modular multistable metamaterial can be tuned by inserting a bar into the unit cells to control the shape of the contrained beams (reproduced from Mao et al., 2022 with permission from Elsevier at `https://doi.org/10.1016/j.engstruct.2022.114976`). **(B)** Origami-based closed-loop units are used as building block, enabling the modular construction of foldable structure with controlled folding kinematics and kinetics (reproduced from Mousanezhad et al., 2017 with permission from Springer Nature due to its open-access status). **(C)** Origami-based metamaterials can be reconfigured into a large number of different shapes with few degrees of freedom, simplifying both actuation and control (reproduced from Li et al., 2024 with permission from Springer Nature due to its open-access status). **(D)** Modular and Uniformly Thick Origami-Inspired Structure (MUTOIS) are able to reconfigure from a compact packaged configuration, to a bus stop or a bridge (reproduced from Zhu and Filipov, 2024 with permission from Springer Nature due to its open-access status).

figurations of individual modules. Additionally, modularity recently attracted attention in the field of sustainable design. Several studies highlight the potential benefits of modularity, such as the possibility to reuse and repair the modules easily to avoid the production of new parts. Modular components are also easier to disassemble for recycling and can be upgraded efficiently (Sonego et al., 2018). A high degree of reparability and adaptability has been demonstrated in large-scale origami-inspired modular structures for civil engineering (Zhu and Filipov, 2024) (see Figure 2.6D).

CHAPTER 3 LITERATURE REVIEW SYNTHESIS AND THESIS OBJECTIVES

Mechanical metamaterials are engineered materials with internal architectures that provide unique mechanical properties rarely found in nature, such as stiffness tunability, shape mophing, and modularity. Due to their capacity to fabricate complex and intricate structures, additive manufacturing techniques are particularly useful to create metamaterials. Multistability, by offering multiple stable states, serves as an effective platform for developing metamaterials with tunable properties.

Although the three properties discussed in the literature review—tunable stiffness, shape morphing, and modularity—have already been investigated in recent studies, they are predominantly developed separately. Metamaterials would greatly benefit from combining these properties, resulting in more versatile functionalities and expanding the range of potential applications. To do so, we propose three objectives :

- **Objective 1 :** Design a unit cell with tunable compressive stiffness, shape morphing abilities, and modularity

  1.1 Study the mechanical response of a building block composed of two combined bistable von Mises trusses

  1.2 Investigate the influence of geometrical parameters on the unit's mechanical properties via finite element analysis and semi-analytical modeling

- **Objective 2 :** Select a fabrication method using 3D printing techniques to characterize experimentally the unit's mechanical properties

  2.1 Fabricate unit cells using Fused Filament Fabrication

  2.2 Test the unit cells in compression to evaluate their effective stiffness variation

- **Objective 3 :** Tesselate the unit cell to create multistable structures with tunable properties

  3.1 Demonstrate the post-fabrication reprogrammability of properties through modularity

  3.2 Create a structure with tunable compressive and bending stiffness

  3.3 Fabricate a sandwich panel with a morphing surface

CHAPTER 4 ARTICLE 1 : EXPLOITING GEOMETRIC FRUSTRATION IN COUPLED VON MISES TRUSSES TO PROGRAM MULTIFUNCTIONAL MECHANICAL METAMATERIALS

Chapter 4 presents the article titled "Exploiting geometric frustration in coupled von Mises trusses to program multifunctional mechanical metamaterials" which has been submitted on August 27, 2024 to Advanced Engineering Materials for the special issue on Additive Manufacturing-Enabled Cellular Materials. It covers the design, fabrication, and modeling of a metamaterial exhibiting tunable stiffness, shape morphing capabilites and modularity. The supplementary information of this article is included at the end of the chapter.

Authors : Yannis Liétard[1,2], Daniel Therriault[1,2,*] and David Mélançon[1,2,*]

[1] Laboratory for Multiscale Mechanics, Department of Mechanical Engineering, Polytechnique Montréal, 2500 Chemin de Polytechnique, Montréal, Québec, H3T 1J4, Canada

[2] Research Center for High Performance Polymer and Composite Systems (CREPEC), Department of Mechanical Engineering, McGill University, 817 rue Sherbrooke Ouest, Montréal, Québec, H3A 0C3, Canada

[*] Corresponding author's emails : david.melancon@polymtl.ca and daniel.therriault@polymtl.ca

4.1 Abstract

Multistable mechanical metamaterials are an emerging class of materials whose intricate internal structure can be engineered to program mechanical properties and promote reversible transitions between multiple stable states of energy. This work presents the design of a mechanical metamaterial based on an assembly of bistable von Mises trusses. We show that coupling two von Mises trusses induces geometric frustration, which leads to an asymmetry between the stable states. We then combine the von Mises trusses to build a unit cell that can change effective stiffness in compression when switching states. Based on a semi-analytical model, we characterize the stiffness variation as a function of the geometric parameters and highlight three possible scenarios: (1) increased, (2) decreased, or (3) constant stiffness between the stable states. To validate the concept, we fabricate our multistable metamaterials out of polylactic acid and thermoplastic polyurethane via fused filament fabrication, and evaluate their mechanical response by measuring experimentally the effective stiffness in both stable states under compression. Our unit cell also features modularity, enabling reversible assembly and post-fabrication tunability. Finally, a range of applications are explored, including sandwich panels capable of changing their compressive and bending stiffness as well as their surface morphology.

4.2 Introduction

Recent advances in the field of mechanical metamaterials have significantly enhanced the tunability of their mechanical properties (Zadpoor, 2016; Bertoldi et al., 2017; Jiao et al., 2023). Among these, stiffness stands out as a particularly important attribute. The manipulation of stiffness has been successfully achieved through various innovative mechanisms, such as origami and kirigami-inspired designs (J. T. Overvelde et al., 2016; Zhai et al., 2020; X. Wang et al., 2023; Yang et al., 2018; Zhai et al., 2018; Fang et al., 2018; Wo and Filipov, 2023; Q. Liu et al., 2023; Silverberg et al., 2014), topological transformations (L. Wu and Pasini, 2023, 2024), and stimuli-responsive materials (Mueller et al., 2022; Jackson et al., 2018; Chen et al., 2021). The capability to tune material stiffness opens up a multitude of applications, including soft grippers (Zhai et al., 2020; Tang et al., 2020), smart fabrics (Y. Wang et al., 2021), structures that soften to prevent damage during collisions (Mintchev et al., 2018), sensing and data transmission (Librandi et al., 2021; Mofatteh et al., 2022), as well as biomimetic robots (Zhong et al., 2021). Another exotic property of mechanical metamaterials is shape morphing, which allows them to be reconfigured and undergo significant and reversible changes in shape (J. T. Overvelde et al., 2016; Coulais et al., 2016; Raviv

et al., 2014; Guseinov et al., 2020; Hwang et al., 2022). Some mechanical metamaterials utilize mechanisms to retain specific shapes without the need for constant actuation (Chen and Shea, 2021; Y. Zhang et al., 2022; Haghpanah et al., 2016; Meeussen and Van Hecke, 2023; De Jong et al., 2023; L. Wu and Pasini, 2023; Risso et al., 2024). These shape morphing capabilities are particularly useful for applications such as aerodynamic drag control (Terwagne et al., 2014), morphing drones and underwater machine (Hwang et al., 2022), or deployable implants for minimally invasive surgery (Bobbert et al., 2020). Moreover, recent research has underscored the importance of modularity, which enables mechanical properties to be tuned post-fabrication (Li et al., 2021; Mao et al., 2022; Li et al., 2024; Zhu and Filipov, 2024), enhancing the versatility and adaptability of mechanical metamaterials.

While these three properties—tunable stiffness, shape morphing, and modularity—have been mostly developed separately, here, we propose a multistable mechanical metamaterial that combines them all. In order to achieve this purpose, we first take inspiration from a simple bistable building block shown in Fig. 4.1A: the von Mises truss. By coupling two independent von Mises trusses, we show that we can tune the amount of geometric frustration to achieve the desired mechanical response (Fig. 4.1B). This is the starting point of a bottom-up strategy leading to multistable unit cells combining four coupled von Mises trusses described in Fig. 4.1C. Our unit cell displays tunable compressive stiffness in its different stable states (Fig. 4.1D), post-fabrication reconfigurability through modularity (Fig. 4.1E), and shape morphing capabilities (Fig. 4.1F). We subsequently utilize these properties to create sandwich panels with adjustable compressive and bending stiffness, as well as morphing surfaces.

4.3 Coupled von Mises trusses exhibiting geometric frustration

Our bistable building block draws inspiration from the von Mises truss, a well-recognized concept employed to achieve bistability (Chi et al., 2022; L. Wu and Pasini, 2024; Chen and Shea, 2021), comprising an assembly of two trusses pinned at their apex and simply supported at their lower ends. A von Mises truss can be characterized by two geometric parameters: θ, representing the initial angle of inclination of the two trusses relative to the horizontal plane, and L, denoting the initial length of one truss. When a displacement δ is applied at its apex, the von Mises truss undergoes a deformation that is characterized by an energy landscape with stable states of identical strain energy level (see Fig. 4.1A). We obtain a similar behavior for all von Mises trusses characterized by $L > 0$ and $\theta \in]0, 90[$. To achieve a broader range of responses, we propose a building block which consists in an assembly of two *coupled von Mises trusses*. These coupled von Mises trusses can be characterized by three geometric parameters forming our design space: (i) θ_{0xy} and (ii) θ_{0xz}, representing the initial angles of

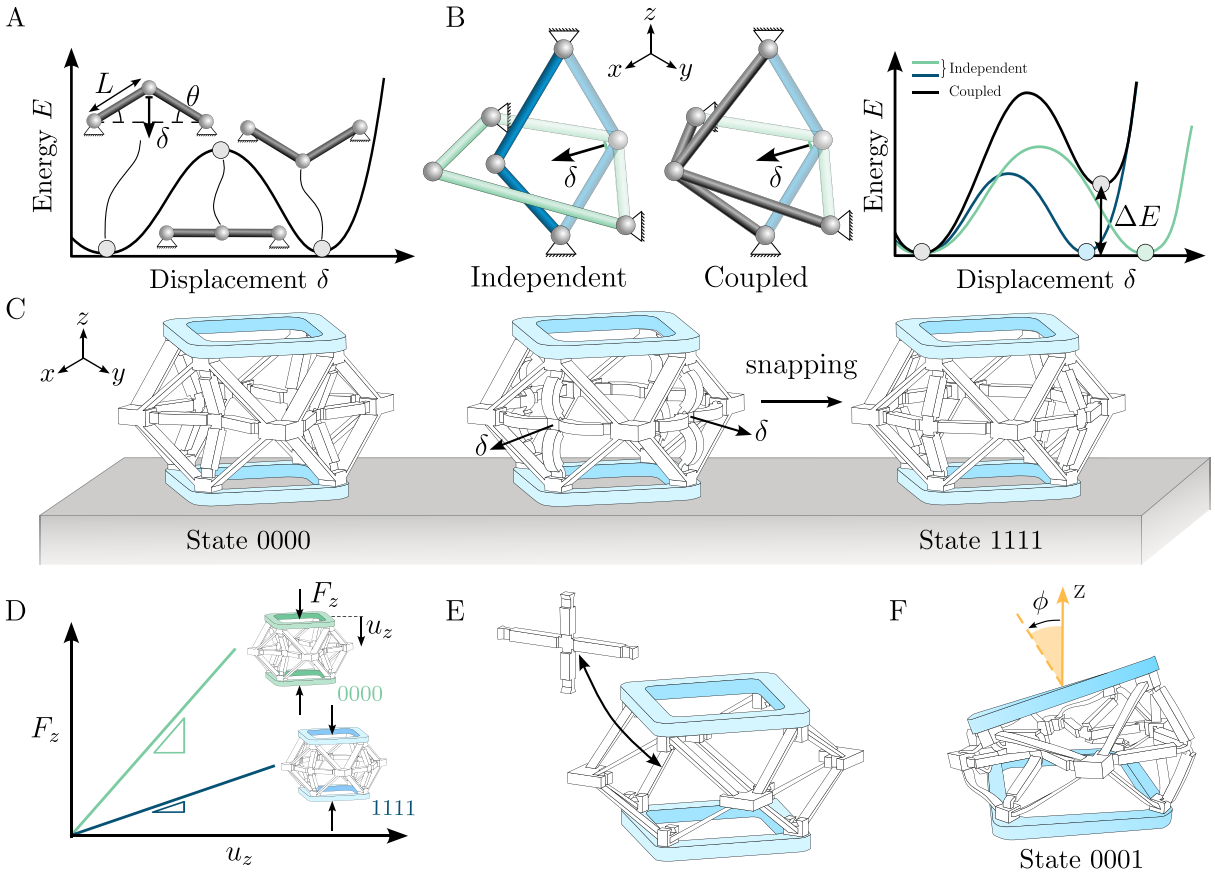

Figure 4.1 | **Multistable mechanical metamaterials capable of stiffness tunability, modularity and shape morphing (A)** A bistable von Mises truss can be characterized by an initial length L and an initial angle θ. The energy landscape of this bistable structure exhibits two energy wells with equivalent strain energy levels. **(B)** When coupled, two von Mises trusses with non-coplanar extremities form a building block that displays geometric frustration in the second stable state, as evidenced by the existence of the energy ΔU in the second stable state. **(C)** Four building blocks are assembled to form a unit cell. Each building block corresponds to a face of the unit and has two stable states, 0 and 1. When all the faces are in the first stable state, the unit is in state 0000, and when all the faces are in the second stable state, the unit is in state 1111. **(D)** Our unit cell is capable of changing stiffness in compression when switching from state 0000 to state 1111. **(E)** The fabrication process of the unit enables reversible assembly of the von Mises trusses, making it possible to easily change the unit's properties post-fabrication. **(F)** When activating only one face in state 0001, the height of this side changes, causing the unit to bend and offering potential for shape morphing applications.

the von Mises trusses in the xy-plane and xz-plane, respectively, and (iii) $r_L = L_{0xy}/L_{0xz}$, the ratio of the initial lengths (see Fig. 4.2A). Another important geometrical characteristic is the distance Δ, defined as the algebraic distance between a first line connecting the two ends of the von Mises truss in the xz-plane and a second line connecting the ends of the von

Mises truss in the xy-plane.

We first characterize the energy landscape of our coupled von Mises trusses by conducting Finite Element (FE) simulations (ABAQUS 2022). Exploiting symmetry, we model one quarter of the structure using beam elements and an incompressible neo-Hookean hyperelastic model with initial Young's modulus E_0 (see section S2 of Supplementary Materials for details). When a displacement δ is imposed on the central node, three distinct scenarios can emerge. First, if the four simply supported nodes lie on the same plane, i.e., for double von Mises trusses characterized by $\Delta = 0$, there is no geometric frustration in the second stable state and there are two zero local minima in the energy-displacement curve (see green curve in Fig. 4.2B). Instead, if the four extremities are not coplanar, i.e., for double von Mises trusses characterized by $\Delta \neq 0$, geometric frustration arises in the second stable state because both von Mises trusses cannot simultaneously minimize their energy (see the blue curve in Fig. 4.2B). Finally, if geometric frustration is too high, the double von Mises truss becomes monostable (see the yellow curve in Fig. 4.2B). The asymmetry induced by geometric frustration between the two stable states can potentially result in distinct mechanical properties. This finding, along with recent research leveraging geometric frustration to design programmable metamaterials (Bertoldi et al., 2017; Silverberg et al., 2014) motivated us to utilize the proposed building block in the construction of a mechanical metamaterial unit.

4.4 Unit cell with tunable mechanical properties

Having demonstrated that coupled von Mises trusses can display geometric frustration in its second stable state, we use it to form a mechanical metamaterial unit cell capable of tuning compressive stiffness (see Fig. 4.3A where each of the four faces of the unit cell corresponds to coupled von Mises trusses). Depending on the state of the unit's faces, i.e., 0000 indicating that all four faces are folded inward and 1111 indicating they are snapped outward, the compressive stiffness may vary. We begin by conducting FE analyses using ABAQUS 2022 to predict the mechanical response in compression of our unit. Taking advantage of the symmetry of the structure, we model a quarter of a unit's face using an unstructured mesh of 8-node linear volumetric elements and an incompressible neo-Hookean hyperelastic model with initial Young's modulus $E_0 = 28$ MPa (see details of the FE simulation in Section S2 of the Supplementary Materials). The stiffness variation, η, is calculated as the ratio of the stiffness in state 1111, K_{1111}, over the stiffness in state 0000, K_{0000}. As revealed by our simulations on the coupled von Mises trusses, we expect no change in compressive stiffness between states 0000 and 1111 for a geometry where the four extremities lie on the same plane, i.e., $\Delta = 0$. We simulate the response of an *iso-stiffness unit* with ($r_L^{iso} = 2.0$, $\theta_{0xy}^{iso} =$

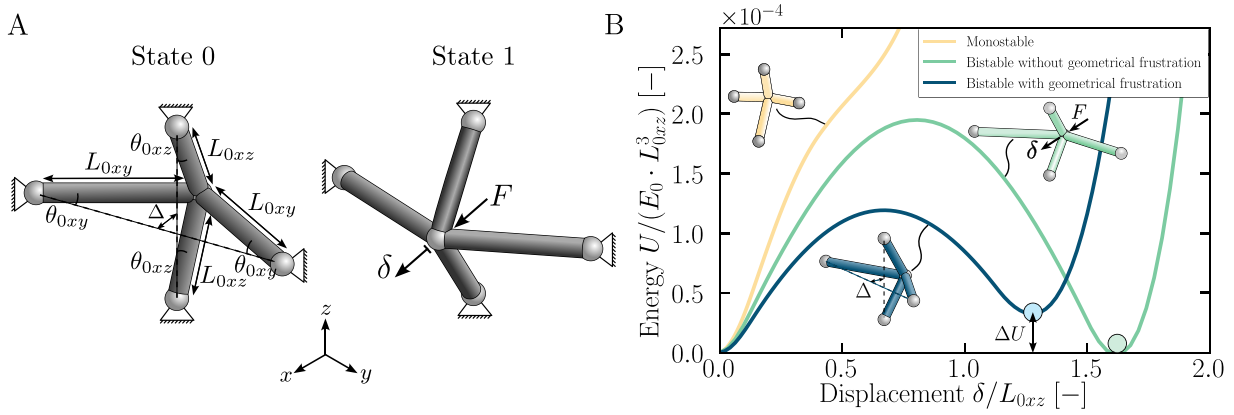

Figure 4.2 | **Building block based on coupled von Mises trusses (A)** The building block can be characterized by three design parameters : the ratio of the initial length $r_L = L_{0xy}/L_{0xz}$ and two initial angles θ_{0xy} and θ_{0xz}. The initial state is denoted as state 0, while the second stable state is referred to as state 1. **(B)** The building block is initially analyzed using a finite element model to characterize the evolution of the normalized elastic energy, $U/(E_0 \cdot L_{0xz}^3)$ as a function of the normalized displacement, δ/L_{0xz} applied at the central vertex. We find three distinct scenarios: monostable (yellow curve), bistable without geometric frustration (green curve), when all four extremities are coplanar, and bistable with geometric frustration (blue curve), when the four extremities are not coplanar. Non-coplanar geometries are characterized by the distance Δ, which is defined as the algebraic distance between a first line connecting the two ends of the von Mises truss in the xz-plane and a second line connecting the ends of the von Mises truss in the xy-plane.

21°, $\theta_{0xz}^{iso} = 40°$) and find similar effective compressive stiffness of $(K_{0000}^{iso})_{FE} = 10.1$ N/mm and $(K_{1111}^{iso})_{FE} = 11.6$ N/mm, in both stable states (see green bars in Fig. 4.3B), resulting in a stiffness variation of $\eta_{FE}^{iso} = 1.15$. Instead, if the four extremities are not coplanar, i.e., $\Delta \neq 0$, geometric frustration in the second stable state will induce a change in compressive stiffness. We consider two additional geometries for which $\Delta < 0$, i.e. ($r_L^{soft} = 2.0$, $\theta_{0xy}^{soft} = 25°$, $\theta_{0xz}^{soft} = 30°$) and $\Delta > 0$, i.e. ($r_L^{stiff} = 2.0$, $\theta_{0xy}^{stiff} = 20°$, $\theta_{0xz}^{stiff} = 55°$). For the first non-coplanar unit, our FE simulations predict a *softening* behavior, with values of the effective compressive stiffness dropping from $(K_{0000}^{soft})_{FE} = 14.2$ N/mm to $(K_{1111}^{soft})_{FE} = 2.18$ N/mm (see blue bars in Fig. 4.3B), yielding a stiffness variation of $\eta_{FE}^{soft} = 0.15$. In contrast, for the second non-coplanar unit, we find a *stiffening* behavior with $(K_{0000}^{stiff})_{FE} = 4.89$ N/mm to $(K_{1111}^{stiff})_{FE} = 20.6$ N/mm (see red bars in Fig. 4.3B), which leads to a stiffness variation of $\eta_{FE}^{stiff} = 4.2$.

To experimentally investigate the compressive stiffness variation of the unit when switching from state 0000 (Fig. 4.3A(i)) to state 1111 (Fig. 4.3A(ii)), we fabricate the *iso-stiffness*, *softening*, and *stiffening* units out of thermoplastic polyurethane (white TPU from Polymaker

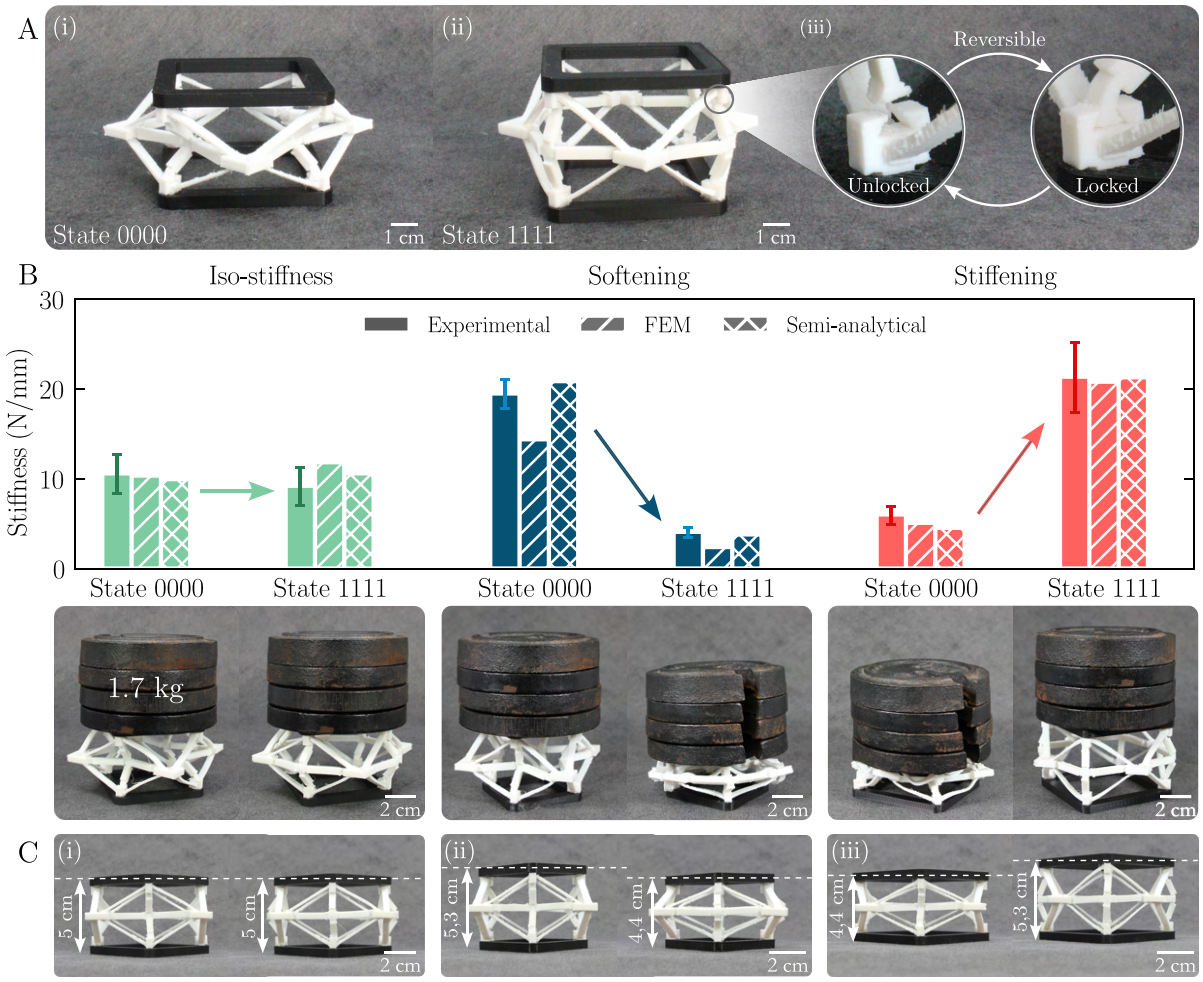

Figure 4.3 | **Tunable mechanical properties (A)** A mechanical metamaterial unit cell consisting of an assembly of four building blocks. (i) When all four faces are in their initial state, this configuration is denoted as state 0000. (ii) Conversely, when all faces are in the second stable state, this configuration is referred to as state 1111. (iii) The coupled von Mises trusses are assembled with an interlocking mechanism that allows for reversible assembly, thereby making the unit modular. **(B)** Three different designs are experimentally tested in compression: an iso-stiffness unit, with no stiffness variation between the two stable states; a softening unit, showcasing decreasing stiffness; and a stiffening unit, demonstrating increasing stiffness. Experimental uncertainties were obtained by repeating the tests on three samples, five times for each sample. **(C)** (i) The iso-stiffness unit does not change height when switching from state 0000 to state 1111, (ii) the softening unit exhibits decreasing height and (iii) the stiffening unit demonstrates increasing height.

with $E_0 = 28$ MPa). Note that we add rigid parts on the top and bottom of the unit to ensure smooth load transfer during mechanical tests (black PLA from Ultimaker). Additional details on the fabrication process can be found in the Section S1 of the Supplementary

Materials. A sliding mechanism is used to fix the coupled von Mises trusses, as presented in Fig. 4.3A(iii), which enables reversible assembly to modify the unit's properties after manufacture. Compression tests are performed (MTS Insight electromechanical machine, MTS Systems Corporation, Eden Prairie, Minnesota, US) with a displacement-controlled load (10 mm/min) in states 0000 and 1111 to evaluate the effective stiffness in compression, which is given by the slope of the force-displacement curve in the linear regime (see Fig. 4.3B). For the *iso-stiffness* unit, the stiffness values in states 0000 and 1111 are $(K^{iso}_{0000})_{exp} = 10.4 \pm 2.15$ N/mm and $(K^{iso}_{1111})_{exp} = 9.01 \pm 2.13$ N/mm, respectively (see green bars in Fig. 4.3B), resulting in a stiffness variation of $\eta^{iso}_{exp} = 0.87$. This minimal stiffness variation is demonstrated visually by placing a weight of 1.7 kg on top of the unit in both stable states in Fig. 4.3B, where no change is observed in the deformation. The experimental results for the *softening* unit reveal a stiffness of $(K^{soft}_{0000})_{exp} = 19.3 \pm 1.62$ N/mm in state 0000 and $(K^{soft}_{1111})_{exp} = 3.88 \pm 0.571$ N/mm in state 1111. Compressive stiffness decreases when all faces are actuated, as evidenced by a stiffness variation of $\eta^{soft}_{exp} = 0.20$. While the unit in the first stable can withstand a weight of 1.7 kg, it fails under the same load in the second stable state (see insets in Fig. 4.3B). Lastly, for the *stiffening* unit, we measure a stiffness of $(K^{stiff}_{0000})_{exp} = 5.82 \pm 1.01$ N/mm in state 0000 and $(K^{stiff}_{1111})_{exp} = 21.2 \pm 3.86$ N/mm in state 1111. The resulting stiffness variation is $\eta^{stiff}_{exp} = 3.64$, confirming that stiffness can increase as well. Whereas the unit yields under a load of 1.7 kg in the first stable state, it can support the same load in the second stable state (see insets in Fig. 4.3B). Overall, for the three geometries studied, the experimental results are in good agreement with the finite element simulations.

In addition to the ability to modify stiffness, the proposed unit cell also demonstrates shape morphing abilities. As illustrated in Fig. 4.3C, the height of a unit can be altered through the actuation of its faces. Similar to the results observed for stiffness variation, three distinct behaviors are identified. For the *iso-stiffness unit*, no height variation is detected. Conversely, for the *softening* unit, the height decreases from 5.3 cm to 4.4 cm when transitioning from the first stable state to the second. Finally, for the *stiffening* unit, the height increases from 4.4 cm to 5.3 cm.

Motivated by the ability to tune stiffness and height, we develop a semi-analytical model to map the stiffness and height variation of the unit across our design space and to gain more insight into the underlying causes of these variations. Our model is based on a combination of axial and torsion springs, to represent the trusses and the joints respectively, along with Euler-Bernoulli beams to model the beams of the frames. The energy of the system in both stable states under compression can be determined by using the principle of minimum potential energy. The corresponding force-displacement curves are then derived by differentiating the energy with respect to displacement. The stiffness in each stable state is calculated as

the initial slope of the force-displacement curves (see details on the semi-analytical model in Section S3 of the Supplementary Materials). This approach enables rapid evaluation of stiffness and height variation. The semi-analytical model's predictions for the stiffness values of the iso-stiffness unit ($(K^{iso}_{0000})_{sa} = 9.74\text{N/mm}, (K^{iso}_{1111})_{sa} = 10.4\text{N/mm}$), the softening unit ($(K^{soft}_{0000})_{sa} = 20.7\text{N/mm}, (K^{soft}_{1111})_{sa} = 3.59\text{N/mm}$) and the stiffening unit ($(K^{stiff}_{0000})_{sa} = 4.32\text{N/mm}, (K^{stiff}_{1111})_{sa} = 21.1\text{N/mm}$) closely align with the experimental results, therefore validating the model (see Fig.4.3B).

We use our semi-analytical model to conduct a parametric study over a design space characterized by $[r_L, \theta_{0xy}, \theta_{0xz}] \in [0.5, 2.0] \times [10°, 70°] \times [10°, 70°]$. For each variable, we use ten linearly spaced points, leading to $1,000$ different geometries. The parametric study reveals various possible scenarios : (1) monostable, (2) no stiffness variation, (3) decreased stiffness, and (4) increased stiffness and height. In particular, Fig. 4.4 shows the influence of the geometrical parameter Δ on the stiffness ratio η (see Fig.4.17B for the influence on height variation). When $\Delta = 0$, the four extremities of the von Mises trusses are coplanar and no stiffness variation is observed. Then, two different behaviors are observed depending on the sign of Δ. With the exception of a few cases, when Δ is negative, the stiffness of the unit decreases when switching from state 0000 to state 1111. In contrast, when Δ is positive, the stiffness increases. The influence of Δ can be explained by the fact that the stiffness of the unit essentially comes from the von Mises trusses in the xz-plane, highlighted in blue and red in the insets of Fig. 4.4. When these trusses are completely vertical (i.e. $\theta_{0xz} = 0°$), they are solicited purely axially, making the unit very stiff. In contrast, when the trusses are inclined (i.e. θ_{0xz} is maximal), resistance is mainly provided by the joints and the unit is very soft. When $\Delta < 0$, the initial angle in the first stable state, θ_{0xz}, is smaller than the angle in the second stable state, θ_{1xz}, (see the highlighted blue trusses in Fig. 4.4) which is why the stiffness decreases. Conversely, when $\Delta > 0$, θ_{0xz} is bigger than θ_{1xz} (see the highlighted red trusses in Fig. 4.4), resulting in an increased stiffness.

The bounds of the stiffness variation can be determined by considering limit cases. The softest configurations are obtained when the value of θ_{0xz} is maximal. By only considering the stiffness of the joints, we can calculate a lower limit of the unit's stiffness $K_{min} = 1.4$ N/mm. The stiffest configurations are obtained when $\theta_{0xz} = 0°$. By only considering the axial stiffness of the vertical von Mises trusses, we find an upper limit $K_{max} = 88$ N/mm (the derivation of K_{min} and K_{max} can be found in Section S3 of the Supplementary Material). Therefore, the stiffness variation is expected to lie within an interval $[K_{min}/K_{max}, K_{max}/K_{min}] = [0.016, 63]$, which is in good agreement with the results given by the semi-analytical model, confirming the predominant role of the initial inclination of the von Mises trusses in the xz-plane on the compressive stiffness of the unit.

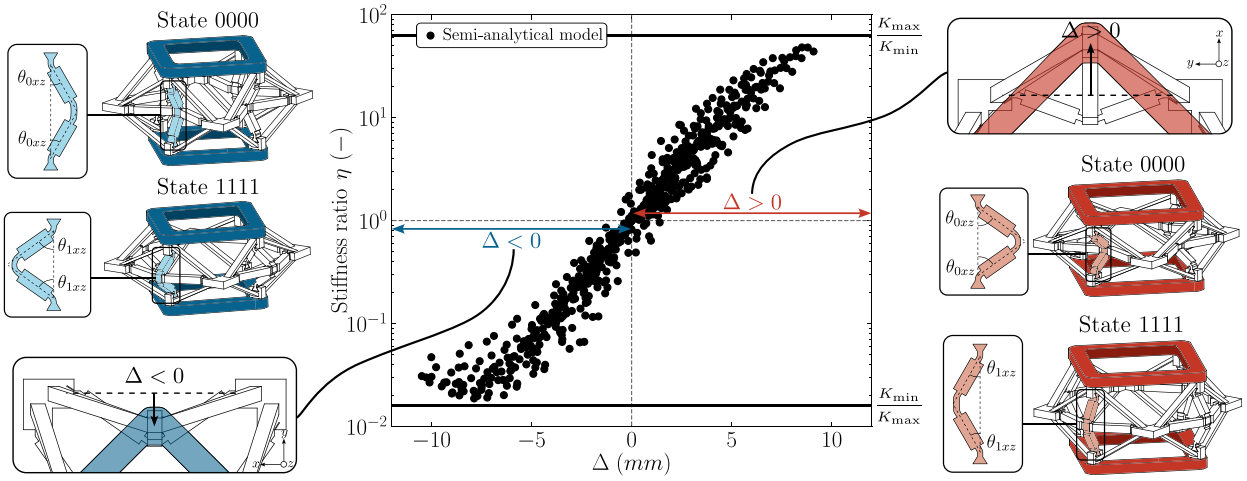

Figure 4.4 | **Evolution of the stiffness ratio as a function of** Δ The paramater Δ is defined as the algebraic distance between a first line connecting the two ends of von Mises truss in the xz-plane and a second line connecting the ends of the von Mises truss in the xy-plane. Through semi-analytical modeling, we show that when $\Delta = 0$, no change in stiffness is observed; however, when $\Delta < 0$, the stiffness decreases, and when $\Delta > 0$, the stiffness increases.

4.5 Post-fabrication modularity

Next, we now show that the reversible assembly process of the unit enables its stiffness variation, η, to be reprogrammed post-fabrication. For this, we start from the *stiffening unit* studied in Fig. 4.3 with $r_L^{stiff} = 2.0$, $\theta_{0xy}^{stiff} = 20°$, $\theta_{0xz}^{stiff} = 55°$, and $L_{0xz}^{stiff} = 10$ mm (see Fig. 4.5A(i)). The coupled von Mises trusses within each face of the unit can be substituted with a new geometry, forming a unit characterized by $r_L^{stiff'}$, $\theta_{0xy}^{stiff'}$, $\theta_{0xz}^{stiff'}$, provided that the new double von Mises truss is able to be attached to the original frame without deforming it (see Section S4 of the Supplementary Materials for details on the geometric compatibility conditions). For example, we find that a double von mises truss characterized by $r_L^{stiff'} = 1.44$, $\theta_{0xy}^{stiff'} = 34°$, $\theta_{0xz}^{stiff'} = 67°$ with $L_{0xz}^{stiff'} = 16$ mm is compatible to the original *stiffening unit*. We 3D print this new unit with thermoplastic polyurethane (blue TPU 95A from Polymaker with $E_0 = 28$ MPa—see Fig. 4.5A(ii)). In Fig. 4.5B, we report the force-displacement curves of the initial geometry (see the grey curves) and the new geometry (see the blue curves) under compression in both stable states. Whereas the original stiffening unit exhibits a stiffness variation of $\eta = 3.6$, the modified one with blue von Mises trusses displays a stiffness variation of $\eta' = 1.5$. While multistability alone enables in situ modification of the unit's effective stiffness in the two stable states, modularity increases tunability by allowing changes in the stiffness variation itself.

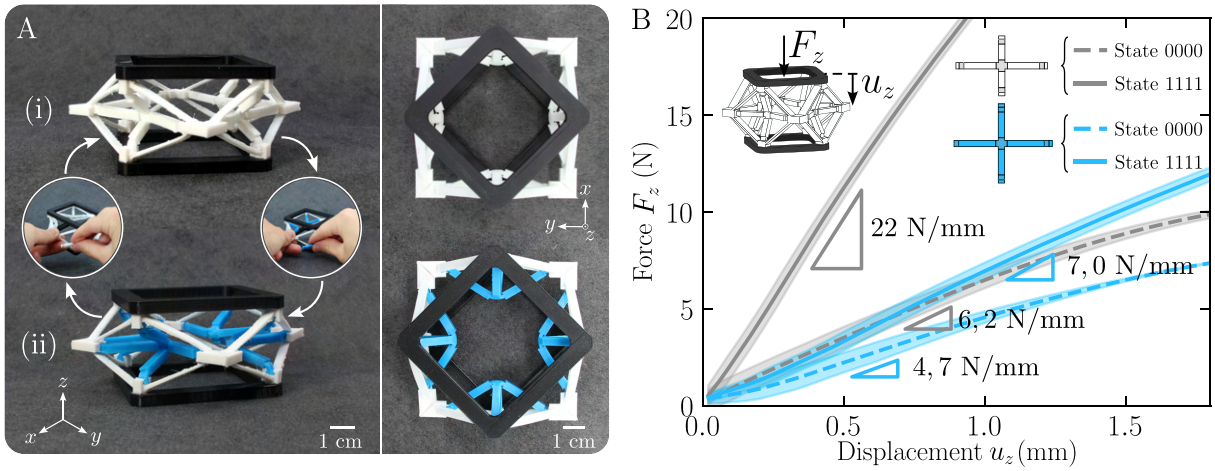

Figure 4.5 | **Post-fabrication reprogramming of stiffness variation through modularity (A)** Using the reversibility of the assembly system described in Fig. 4.3A(iii), we start from the stiffening unit pictured in (i) ($r_L = 2.0$, $\theta_{0xy} = 20°$, $\theta_{0xz} = 55°$) and obtain the unit shown in (ii) ($r_L = 1.44$, $\theta_{0xy} = 35°$, $\theta_{0xz} = 69°$) by replacing the coupled von Mises trusses within each face. **(B)** This change in geometry results in a modification of the stiffness variation, as evidenced by the compression tests conducted. The experimental uncertainty is obtained by repeating the tests in compression five times.

4.6 Tunable sandwich panel

We exploit the stiffness tunability of our mechanical metamaterial unit cell to build a sandwich panel displaying distinct compressive and bending stiffness. The panel is composed of six units enclosed between two acrylic plates (see Fig. 4.6A). We select a unit exhibiting a significant height variation, which also proves to have a substantial change in stiffness. The process used to determine its geometry ($r_L^{sandwich} = 1.14$, $\theta_{0xy}^{sandwich} = 28°$, $\theta_{0xz}^{sandwich} = 58°$) is described in the Section S4 of the Supplementary Materials. The unit is fabricated in six samples, which can be fixed in a reversible manner between two acrylic plates (see Fig. 4.6A). First, we demonstrate in Fig. 4.6B that the panel's compressive stiffness increases when all units are switched from state 0000 to state 1111. Indeed, as the stiffness in compression of a single unit increases when switching from state 0000 to state 1111 and since six units are combined in parallel, the effective compressive stiffness of the panel increases as well, starting at $K_{0000}^{sandwich} = 45.4$ N/mm when all units are in state 0000 and rising to $K_{1111}^{sandwich} = 70.8$ N/mm.

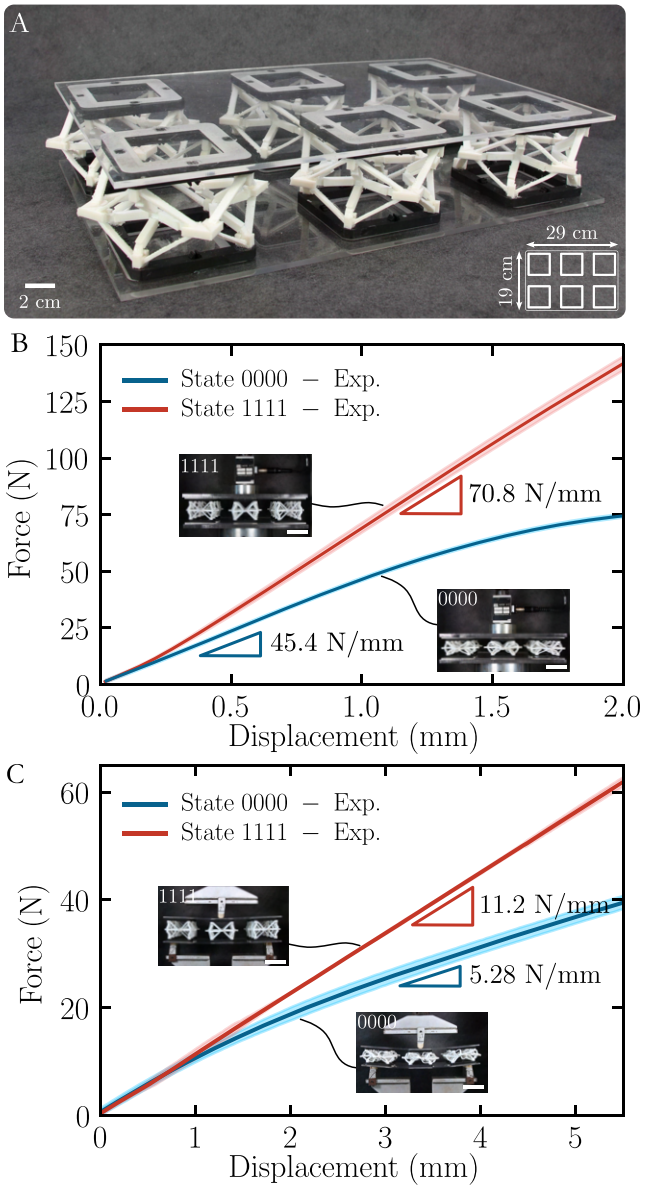

Figure 4.6 | **Application as a sandwich panel with tunable compressive and bending stiffness (A)** The sandwich panel consists of an array of six units fixed between two acrylic plates. **(B)** By performing a compression test, we demonstrate its capability to change compressive stiffness (scale bar is 5 cm). **(C)** The three-point bending test reveals its ability to change bending stiffness (scale bar is 5 cm). The experimental uncertainty is obtained by repeating the tests in compression and bending five times.

The compressive stiffness measured for one unit is $K_{0000}^{unit} = 10.9$ N/mm in state 0000 and $K_{1111}^{unit} = 14.9$ N/mm. As the six units are arranged in parallel, the expected stiffness of the panel are $6 \times K_{0000}^{unit} = 65.4$ N/mm in the first stable state and $6 \times K_{1111}^{unit} = 89.4$ N/mm in the second stable state. However, the experimentally measured values are significantly lower

than these calculated predictions. This discrepancy is likely due to potential imperfections in the manufacturing of the units and the assembly of the panel. In addition to the compressive stiffness variation, two parallel phenomena lead to an increase in bending stiffness when switching from the first stable state to the second one. First, the core of the sandwich panel is stiffer when all the units are in state 1111 compared to state 0000. Second, as each unit's height increases by 18% upon actuation, the sandwich panel's overall thickness also increases, thereby redistributing the constituent material about the neutral axis and enhancing its second moment of area. By conducting a three-point bending test, we confirmed that the panel's bending stiffness increased from 5.28 N/mm when all units are in state 0000 to 11.2 N/mm when all units are in state 1111 (see Fig. 4.6C).

4.7 Surface morphing

Lastly, we fabricate a second sandwich panel consisting of an array of nine units, with an acrylic bottom surface and a top surface made of a thin 3 mm layer of ethylene propylene diene monomer (EPDM) rubber to allow deformation. As the height of a unit can change when transitioning between stable states, actuating only one face allows the unit to bend about the axis perpendicular to its normal (see Fig. 4.1F). To show that this enables control over the curvature of the top surface about the x and y axes, i.e., κ_x and κ_y, respectively, we consider two types of units with different geometries, denoted α and β. Importantly, these units are selected to maximize height variation while meeting two conditions. First, both units must be interchangeable, so that one can be replaced by the other to allow for adjustments in the achievable shapes of the panel. Second, to ensure continuity, unit β is chosen such that its height in state 0000 matches the height of unit α in state 1111. The process followed to select each unit geometry is detailed in Section S4 of the Supplementary Materials. In Fig. 4.7, we highlight with green and blue squares the α and β units on schematics representing three different 3×3 arrangements of the sandwich panel. By selectively actuating different faces, we demonstrate that, depending on the geometry of the units, we can transition from a flat surface (Fig. 4.7A) to different programmed shapes. First, by placing a unit α in the center and surrounding it with eight unit β, the height at the center of the panel can be reduced by switching unit α from the second stable state to the first. Simultaneously, the height at the edges can be increased by actuating the sides of the unit β in the corners of the panel, resulting in a bowl-shaped surface (Fig. 4.7B). Next, we position two units α in the middle of two opposite sides of the panel. By deactivating the outward-facing sides of both unit α, we can induce a negative curvature along the x axis and, by activating the outward-facing sides of unit β, we can induce a positive curvature along the y axis, creating a saddle-shaped surface

(Fig. 4.7C). Finally, we place three units α in the center line along the x axis and six units β on the sides. By deactivating the faces of all unit α and by actuating the outward-facing sides of unit β, we create a zero curvature along the x axis and a positive curvature along the y axis, resulting in a cylindrical shape (Fig. 4.7D). Although the top surface adapts well to the inclination of the unit cells, folds can appear when the curvature is positive. Negative curvature is also limited because the top surface is being stretched. These effects could be mitigated by using a softer material for the top surface and by increasing the number of units in the array to achieve a smoother surface.

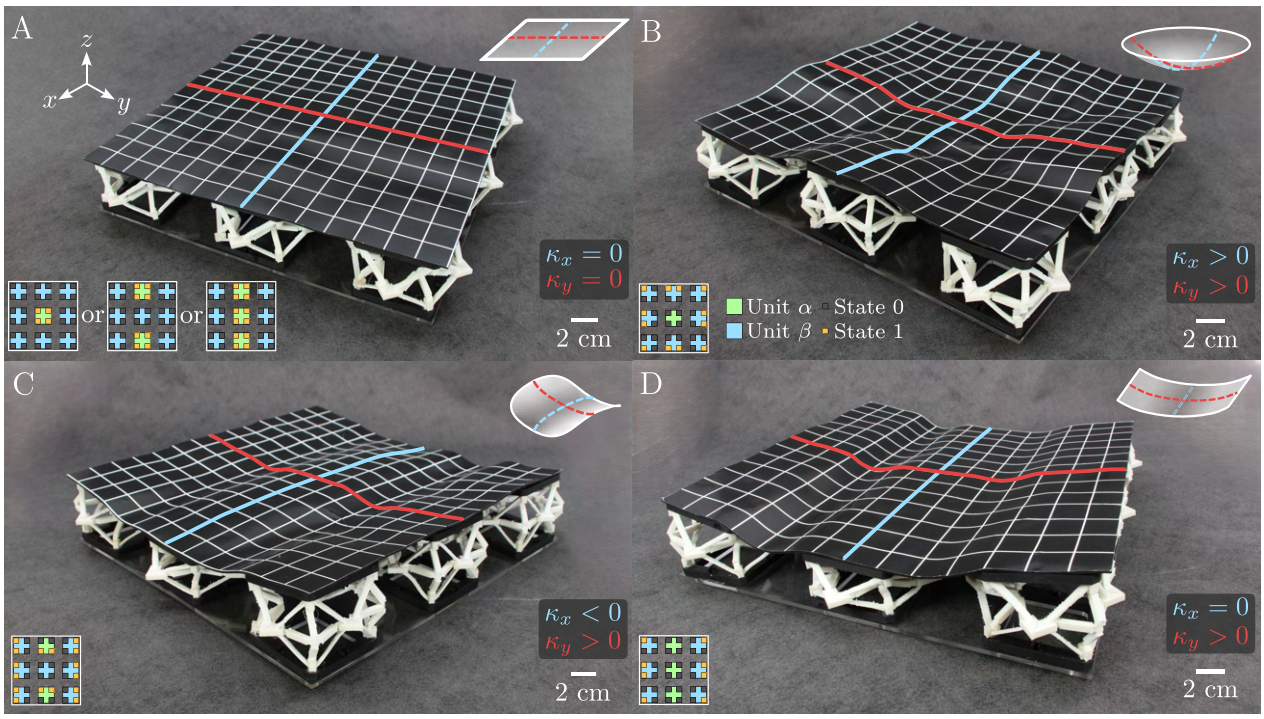

Figure 4.7 | **Application as a sandwich panel with morphing surfaces (A)** Initially, the surface of the sandwich panel is flat. Two types of units with distinct geometries are utilized, designated as α and β. By selectively actuating the faces of the units, different shapes are obtained depending on the geometry of the units : **(B)** a bowl, **(C)** a saddle surface, **(D)** a cylindrical surface. A white grid has been added on the top surface to better visualize its 3D deformation.

4.8 Conclusions

In summary, we introduced a multistable mechanical metamaterial that leverages geometric frustration arising from the assembly of two coupled von Mises trusses to achieve in situ stiffness tunability, shape morphing capabilities, and modularity. By modeling our unit cell both with finite element methods and semi-analytical approaches, we identified various

possible behaviors within distinct regions of our design space: (1) monostability, (2) no stiffness and height variation, (3) decreasing stiffness and height, and (4) increasing stiffness and height. Experimental validation was performed using 3D printed prototypes, resulting in the development of several applications. These include demonstrating the post-fabrication reprogrammability of stiffness variation through the unit's modularity, creating a sandwich panel with tunable compressive and bending stiffness, and designing a sandwich panel capable of morphing a surface.

While this work primarily focused on the design and fabrication of the mechanical metamaterial, manual actuation is still required. Future work should explore remote actuation to enhance ease of use and broaden application potential, which can be achieved through the use of materials responsive to temperature (Mueller et al., 2022; Niknam et al., 2022), magnetic fields (Chen et al., 2021; Ramachandran et al., 2016; Jackson et al., 2018), light (Shankar et al., 2013), using pneumatic actuation (Melancon et al., 2021, 2022; Gorissen et al., 2020; Rahman et al., 2023) or shape memory alloys (Barbarino et al., 2013). Moreover, various multimaterial fabrication techniques (Zhou et al., 2023) could be employed to improve the manufacturing process by reducing the number of parts to assemble and decreasing the scale of the unit cell, thereby expanding the range of potential applications.

We believe that the major advance of the proposed concept lies in its combination of multiple functionalities, namely stiffness tunability, shape morphing, and modularity. The integration of these versatile attributes within a single unit showcases its potential to impact current mechanical metamaterial design, paving the way for innovative solutions in diverse engineering fields such as aerospace, automotive, and biomedical industries, where adaptive materials can significantly enhance performance and efficiency.

4.9 Materials and Methods

The design, materials, and fabrication methods are summarized in Supplementary Materials, Section S1. Details on the FE simulations are provided in Section S2 of the Supplementary Materials. The semi-analytical model is detailed in Supplementary Materials, Section S3. The process for selecting the different unit geometries for the applications is described in Section S4 of the Supplementary Materials.

4.10 Acknowledgments

Funding: We acknowledge support from the Natural Sciences and Engineering Research Council of Canada. **Author contributions:** Y.L., D.T., and D.M. proposed and developed

the research idea. Y.L. designed and fabricated the unit cells and the sandwich panels, performed experiments, developed the semi-analytical model and conducted the numerical simulations. Y.L., D.T. and D.M. wrote the paper. D.T. and D.M. supervised the research. All authors thank Nina Tricot for her assistance with sample fabrication and experimental testing. **Competing interests:** The authors declare no conflict of interest. **Data and materials availability:** The data that support the findings of this study are available on request from the corresponding author.

4.11 Supplementary information : Section S1.Fabrication of unit cells

A unit cell is constituted of four coupled von Mises trusses, four frames, a top and a bottom part. All components are 3D printed individually using an Ultimaker 3 and then glued together except for the von Mises trusses which are assembled using a sliding mechanism enabling reversible assembly. The flexible parts (in white on Fig. 4.8) are printed with white thermoplastic polyurethane (TPU 95A, Ultimaker). The printing speed is 25 mm/s, the printing temperature is 225°C and the infill percentage is 100%. The rigid parts (in black on Fig. 4.8) are printed with polylactic acid (PLA). The printing speed is 60 mm/s, the printing temperature is 210°C and the infill percentage is 100%. The values used for the geometric parameters are : $W = 4$ mm, $l_j = 3$ mm and $t_j = 1.5$ mm. To manufacture a prototype, we follow the steps described below, which are also illustrated on Fig. 4.9 :

- **Step 1 :** We 3D print (Ultimaker 3) each part out of polylactic acid (Ultimaker PLA) and thermoplastic polyurethane (Polymaker TPU 95A), and then fix the von Mises trusses to the frame using the interlocking mechanism.
- **Step 2 :** We glue the four frames.
- **Step 3 :** We glue the top and bottom parts to form a unit cell.

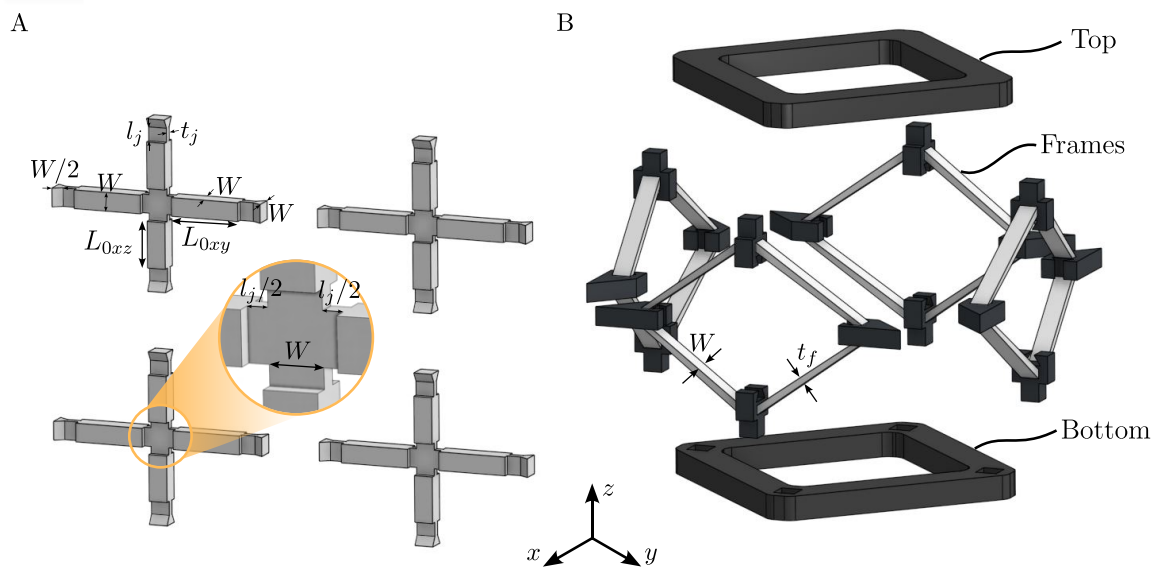

Figure 4.8 | **Design of a unit cell (A)** The coupled von Mises trusses are 3D printed flat with TPU. **(B)** The top and bottom parts are printed out of PLA while the frames are printed using both TPU and PLA for the notch enabling the assembly of the von Mises trusses.

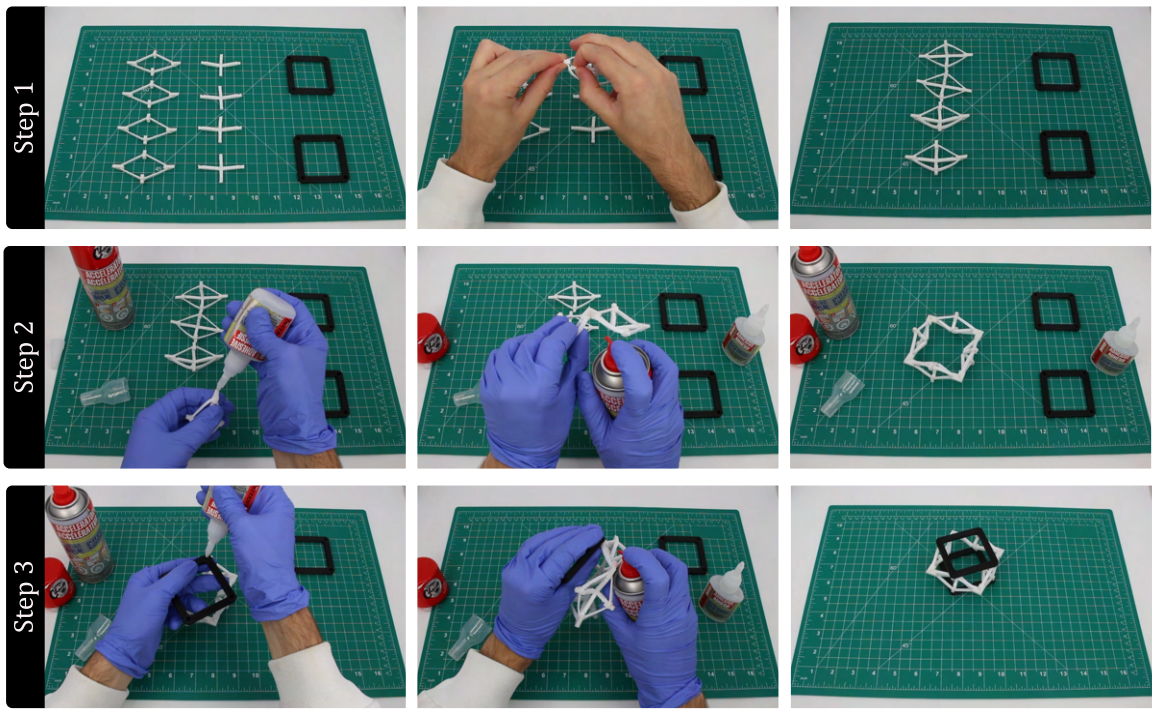

Figure 4.9 | **Fabrication of a unit cell** Snapshots of the unit cell fabrication process

4.12 Supplementary information : Section S2. Finite element simulations

4.12.1 Double von Mises trusses

We conduct finite element simulations of the double von Mises truss to investigate its mechanical response upon actuation. We take advantage of the structure's symmetry and create a 3D model of a quarter of the structure, which is then discretized using beam elements (element type B31 in ABAQUS). The neo-Hookean hyperelastic model is used to describe the constitutive relation of the base material ($E_0 = 27.6$ MPa and $\nu = 0.48$ leading to $C_{10} = 4.66$ MPa and $D_1 = 8.70 \times 10^{-3}$ MPa^{-1}). The Static/General solver with the NLGEOM parameter is used. The three steps of the simulation are described below and illustrated in Fig. 4.10:

- **Step 1 - Assembly.** To reproduce the assembling method used during the fabrication, the coupled von Mises trusses are initially flat. By applying displacement at its extremities, we assemble the coupled von Mises trusses to the frame. The center is fixed during this step.
- **Step 2 - Relaxation.** The ends of the von Mises trusses are clamped and we let the structure relax to simulate what happens experimentally.
- **Step 3 - Transition from state 0 to state 1.** A displacement u_x along the x axis is applied at the center of the von Mises trusses. From this last step, we extract the strain energy as a function of u_x.

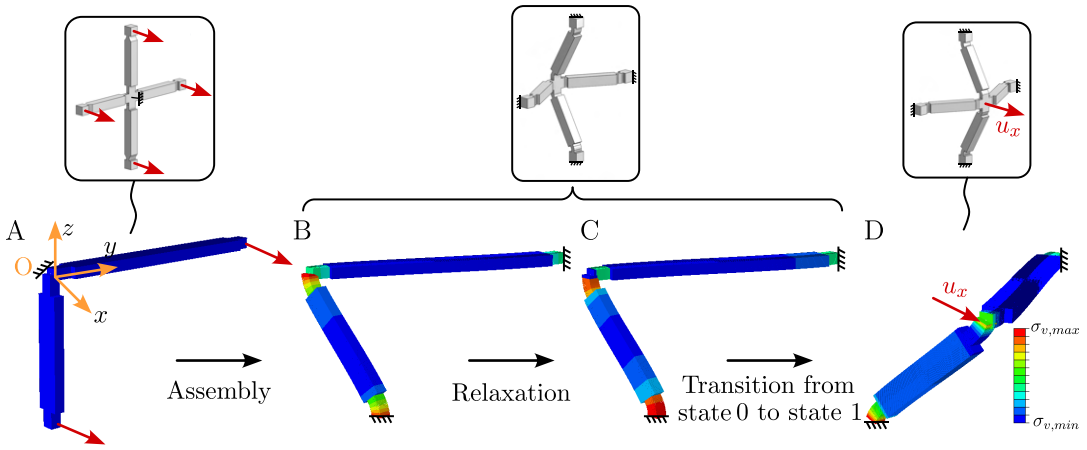

Figure 4.10 | **Simulation of coupled von Mises trusses (A)** In the initial state, the trusses are flat. **(B)** The double von Mises trusses are assembled on the frame which is not modeled here because it is considered infinitely rigid. **(C)** The strucure is relaxed. **(D)** The second stable state is reached.

4.12.2 Unit cell

A similar model is used to study the unit cell, but with different boundary conditions. To remove the rigid body translations and rotations, and take into account the symmetry of the unit, we impose the following set of boundary conditions. For the nodes belonging to the Oxy plane, the translation along y and the rotations around the x and z axis are blocked. For the nodes belonging to the Oxz plane, the translation along y and the rotations around the x and z axis are blocked. The nodes belonging to the extremity of the horizontal von Mises truss can only translate along a line passing through the center of the unit and the initial position of this extremity. Several simulations are performed one after the other and illustrated in Fig. 4.11 :

- **Simulation 1.** To reproduce the assembling method used during the fabrication, the coupled von Mises trusses is initially flat. By applying displacement at its extremities, we assemble the coupled von Mises trusses to the frame.
- **Simulation 2.** The prestress field and resulting deformed geometry thus obtained are imported in a second model. We now use MPC to tie the extremities of the coupled von Mises trusses to the frame. In a first step, we let the structure relax. In a second step, we then apply a displacement at the center of the double von Mises truss. Using this simulation, we derive the energy curve to determine if the structure is bistable. If bistability is observed, we identify the positions of secondary stable states. If the structure is monostable, we conclude the analysis at this stage.
- **Simulation 3.** Starting again from the imported deformed geometry and prestress field of the assembly step, we initiate the process with a relaxation step to allow the structure to settle. Subsequently, in the second step, we induce a transition from the initial stable state to the second stable state by applying a displacement at the center of the double von Mises truss. This is followed by another relaxation step in the third phase. Finally, in the last step, we simulate the compression of the unit by applying a vertical displacement at the end of the von Mises truss in the $xz-$plane. By extracting the reaction force at the nodes where the displacement is applied, we generate a force-displacement curve. The stiffness of the unit in the second stable state corresponds to the slope of this curve.
- **Simulation 4.** We repeat the same process in the first stable state (Step 1 : relaxation, step 2 : compression)

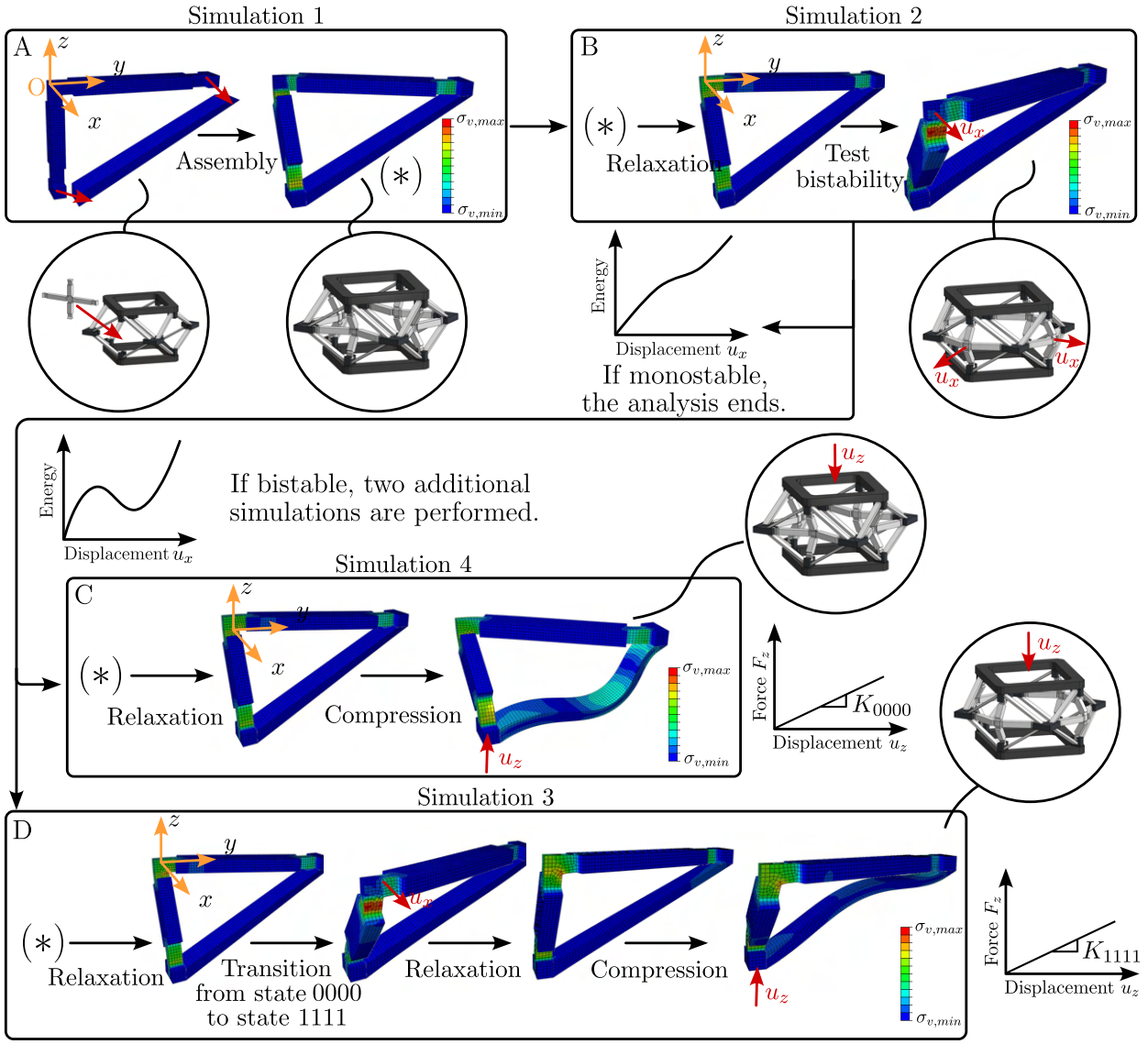

Figure 4.11 | **Three-dimensional simulations of a unit cell (A)** The double von Mises trusses are assembled on the frames of the unit. **(B)** The symbol $(*)$ indicates that the deformed geometry and the stress field are imported from the first simulation in a new model. We let the structure relax and then apply a displacement along the x axis. By extracting the energy curve, we determine if the unit is bistable or not, in which case the analysis stops here. **(C)** The deformed geometry and the stress field are imported from the first simulation. After a relaxation step, we apply a displacement to compress the unit along the z axis. The slope of the force-displacement curve in the linear regime corresponds to the stiffness of the unit in the first stable state. **(D)** We again import the deformed geometry and the stress field of the first simulation, then let the structure relax, apply a displacement along the x axis to reach the second stable state and let the structure relax again. Finally, a displacement along the z axis is applied to compress the unit and evaluate the stiffness in the second stable state.

4.13 Supplementary information : Section S3. Semi-analytical model

Transition from state 0000 to 1111

To conduct a parametric study of the stiffness ratio as a function of $r_L, \theta_{0xy}, \theta_{0xz}$, we build a semi-analytical model based on a set of axial springs (see Fig. 4.12). The top and bottom parts are assumed infinitely rigid, and thus do not contribute to the energy of the system. We take advantage of the symmetry of the structure and focus on one fourth of a face. The von Mises trusses are predominantly loaded axially. Thus, their axial deformation can be described using axial springs with stiffness $k_{xy} = E_0 A_T / L_{0xy}$ for the von Mises truss in the $xy-$plane and $k_{xz} = E_0 A_T / L_{0xz}$ for the von Mises truss in the $xz-$plane, where $A_T = 16$ mm^2 is the cross-sectional area of the trusses. Segment AB, representing a beam within the frame, experiences primarily tension when transitioning between states and is represented by a spring with stiffness $k_F = E_0 A_F / L_{0F}$ ($A_F = 4$ mm^2). We use the following boundary conditions to ensure that this quarter of a face can be representative of the unit : the point A can only translate along the z axis, the point O can only translate along the x axis (see Fig. 4.12A) and the point B can only translate along a line passing through the initial position of the point B and the center of the unit to maintain symmetry between each face (see Fig. 4.12B).

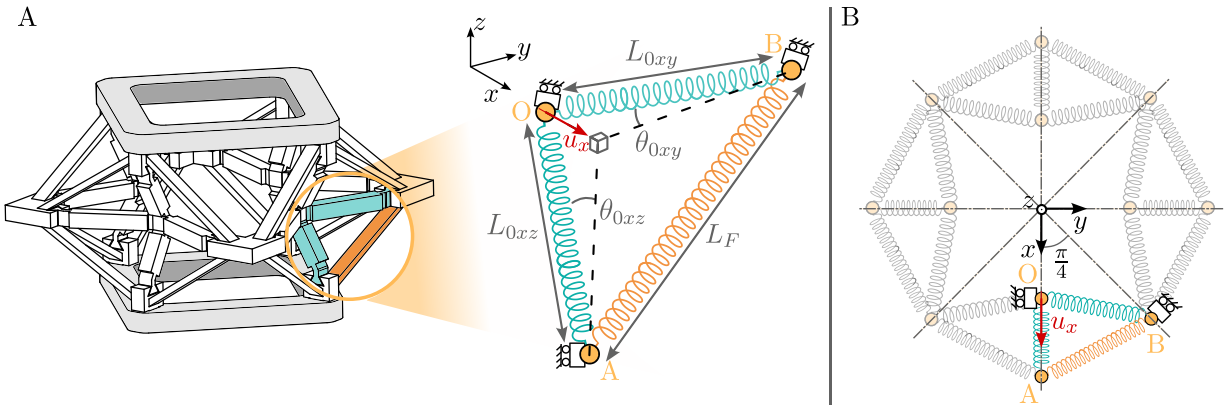

Figure 4.12 | **Semi-analytical model of a unit cell transitioning between the two stable states (A)** Schematic of the springs used to analyse the transition from state 0000 and 1111. **(B)** Top view of the unit representing the boundary conditions used to take into account the unit's symmetry.

The length of the springs can be expressed as a function of a control parameter u_x, which is the displacement along the x axis of the point O, and two degree of freedom θ_{xy} and θ_{xz} corresponding to the angles of the trusses in the $xy-$plane and the $xz-$plane respectively.

L_{xz} and L_{xy} are the length of the trusses in the $xz-$plane and the $xy-$plane respectively. L_F is the length of the frame beam, and L_{0F} is the initial length of the frame beam.

$$L_{xz} = \frac{(L_{0xz} + l_j)\sin(\theta_{0xz}) - u_x}{\sin(\theta_{xz})} - l_j \quad (l_j = 3\text{mm is the length of the joints}), \tag{4.1}$$

$$L_{xy} = \frac{(L_{0xy} + l_j)\cos(\theta_{0xy}) + \tan(\pi/4)(u_x - (L_{0xy} + l_j)\sin(\theta_{0xy}))}{\cos(\theta_{xy}) - \tan(\pi/4)\sin(\theta_{xy})} - l_j, \tag{4.2}$$

$$L_F = \sqrt{\begin{array}{c}[-(L_{0xz} + l_j)\sin(\theta_{0xz}) + u_x + (L_{xy} + l_j)\sin(\theta_{xy})]^2 + \\ (L_{xy} + l_j)^2\cos^2(\theta_{xy}) + (L_{xz} + l_j)^2\cos^2(\theta_{xz})\end{array}}, \tag{4.3}$$

$$L_{0F} = \sqrt{(L_{0xy} + l_j)^2 + (L_{0xz} + l_j)^2 - 2(L_{0xy} + l_j)\sin(\theta_{0xy})(L_{0xz} + l_j)\sin(\theta_{0xz})}. \tag{4.4}$$

The total energy of a unit, noted Π, can be calculated as the sum of the axial springs energy (U_H, U_V and U_F). Each energy is expressed in the following manner :

$$U_{xy} = 4k_{xy}(L_{xy} - L_{0xy})^2, \tag{4.5}$$

$$U_{xz} = 4k_{xz}(L_{xz} - L_{0xz})^2, \tag{4.6}$$

$$U_F = 8k_F(L_F - L_{0F})^2, \tag{4.7}$$

$$\Pi(\theta_{xy}, \theta_{xz}) = U_{xy} + U_{xz} + U_F. \tag{4.8}$$

To determine if a unit is multistable, we apply a displacement u_x at the point O. At each step, u_x increase and the energy of the structure is calculated as a function of θ_{xy} and θ_{xz}. These two degree of freedom can be fixed by applying the principle of minimum potential energy ($\partial\Pi/\partial\theta_{xy} = \partial\Pi/\partial\theta_{xz} = 0$). Thus, we obtain the energy-displacement curve corresponding to the transition between state 0000 and 1111 and, in particular, the position of the second stable state. From the position of the second state, we can deduce the height of the unit in the second stable state and therefore the height variation. Fig. 4.13 shows that, compared to the FE analysis, the semi-analytical model slightly overestimates the elastic energy of the unit during the transition between the two stable states. This discrepancy is due to the fact that springs can only be deformed axially, whereas beams can bend, allowing for a lower energy pathway. Nevertheless, we note a very good agreement between the two models regarding the position of the second stable state, which is the critical information needed in the next step to evaluate the effective stiffness in both stable states.

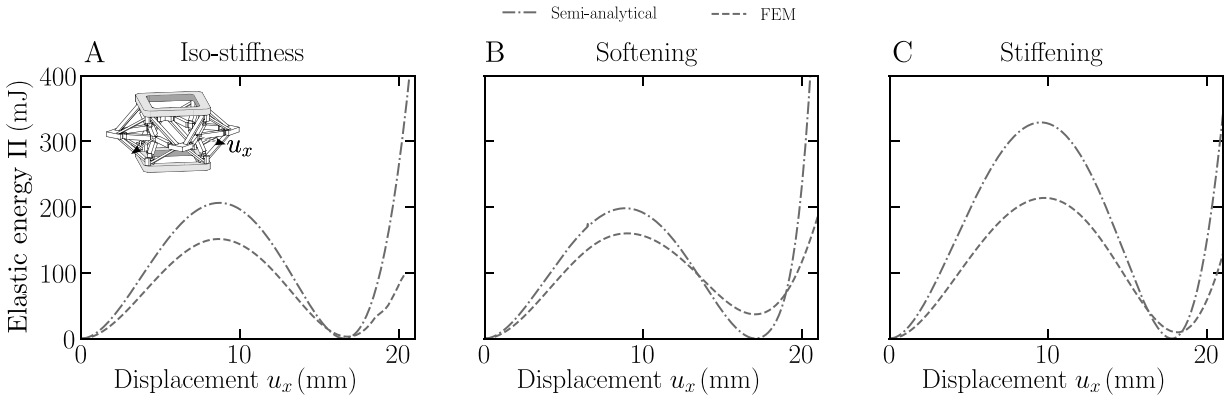

Figure 4.13 | **Comparison of the energy curves obtained with the semi-analytical model and FE simulations** The energy curves correspond to the transition between the two stable states for **(A)** the iso-stiffness unit, **(B)** the softening unit, and **(C)** the stiffening unit.

4.13.1 Compressive stiffness in state 0000 and 1111

In the case of a multistable unit, an additional investigation is conducted to determine the stiffness in state 0000 and state 1111. The previous set of boundary conditions remains applicable, with the exception of point B, which is now clamped to simplify the analysis. The beam corresponding to the frame, which was modeled by a linear spring, is now represented by an Euler-Bernoulli beam, as its deformation is not axial under compression (see Fig. 4.14A). The joints are modeled as torsion springs with a constant k_j or $2k_j$ (see Fig. 4.14B).

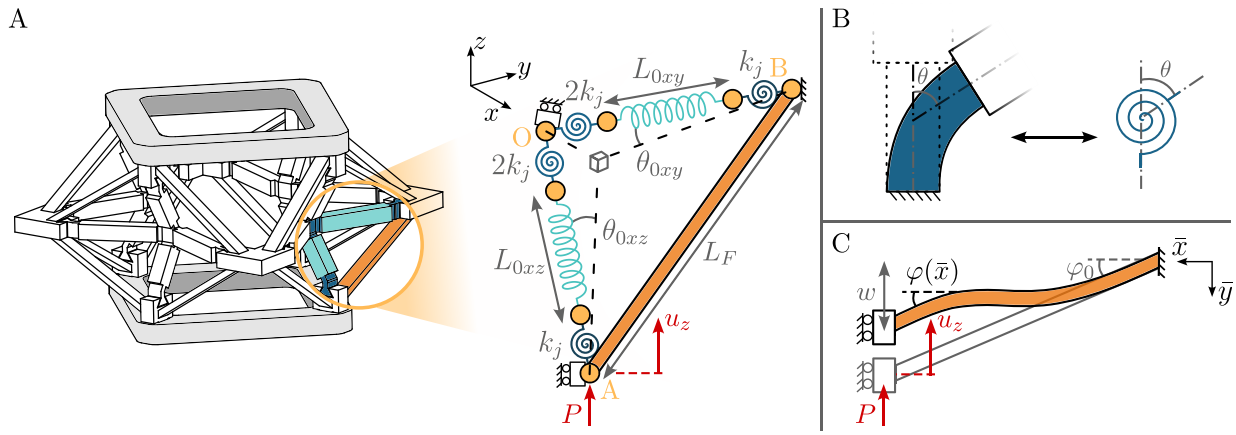

Figure 4.14 | **Semi-analytical model of a unit cell in compression (A)** Schematic of the discretized model used to evaluate the stiffness in compression in state 0000 and 1111. **(B)** The joints are represented by a torsion spring with a constant K_j. **(C)** The beams of the frame are modelled by an Euler-Bernoulli beam.

L_{xy}, L_{xz} and θ_{xy} can be expressed as a function of the control parameter u_z, which is the displacement along the $z-$axis applied at the point A, and a degree of freedom θ_{xz} :

$$\theta_{xy} = \arctan\Bigg(\frac{1}{(L_{0xy}+l_j)\cos(\theta_{0xy})} \left([(L_{0xz}+l_j)\cos(\theta_{0xz}) - u_z]\tan(\theta_{xz}) \right. \\ \left. +(L_{0xy}+l_j)\sin(\theta_{0xy}) - (L_{0xz}+l_j)\sin(\theta_{0xz})\right) \Bigg), \tag{4.9}$$

$$L_{xy} = \frac{(L_{0xy}+l_j)\cos(\theta_{0xy})}{\cos(\theta_{xy})} - l_j, \tag{4.10}$$

$$L_{xz} = \frac{(L_{0xz}+l_j)\cos(\theta_{0xz}) - u_z}{\cos(\theta_{xz})} - l_j. \tag{4.11}$$

When the unit is under compression, the beam of the frame undergoes non-axial deformation, necessitating the use of Euler–Bernoulli beam theory instead of an axial spring. Utilizing this theory, the incremental rotation $\psi(\bar{x}) = \varphi(\bar{x}) - \varphi_0$ (see Fig. 4.14C) can be expressed as :

$$\psi(\bar{x}) = \frac{PL_{0F}^2}{2EI}\left[\left(\frac{\bar{x}^2}{L_{0F}^2}\right) - \left(\frac{\bar{x}}{L_{0F}}\right)\right]. \tag{4.12}$$

We can then deduce the expression for the deflection w :

$$w = \int_0^{L_{0F}} \sin(\varphi(\bar{x}))dx = \int_0^{L_{0F}} \sin(\varphi_0 + \psi(\bar{x}))dx, \tag{4.13}$$

$$\text{where} \quad \varphi_0 = \arccos\left(\frac{\sqrt{L_{0xy}^2 + L_{0xz}^2\sin^2(\theta_{0xz}) - 2L_{0xy}L_{0xz}\sin(\theta_{0xy})\sin(\theta_{0xz})}}{L_{0F}}\right). \tag{4.14}$$

And the energy of the frames is :

$$U_F = 16\int_0^{L_{0F}} \frac{M^2}{2EI}d\bar{x} = \frac{2P^2L_{0F}^3}{3EI}. \tag{4.15}$$

To calculate U_F, we can determine the force P using the expression for deflection. Given the applied displacement u_z, the deflection is known and we can solve for P. Additionally, the joints also offer some resistance due to bending. To account for this bending energy, we model them with torsion springs having a stiffness k_J. By fitting the model to experimental results for the softening unit, we were able to determine the value of k_J and the Young's modulus of TPU 95A E_0 : $k_J = 38.4$ N mm/rad, $E_0 = 27.6$ MPa. The bending energy of the

joints is :

$$U_J = 12k_J[(\theta_{xy} - \theta_{0xy})^2 + (\theta_{xz} - \theta_{0xz})^2]. \tag{4.16}$$

The horizontal and vertical von Mises truss are still represented by springs as previously such that the total energy Π becomes :

$$\Pi(\theta_{xz}) = U_{xy} + U_{xz} + U_F + U_J. \tag{4.17}$$

The energy is then calculated when a displacement u_z is applied at the point A, in both stable states 0000 and 1111. With point B now clamped, the total energy can be expressed as a function of θ_{xz} only. This degree of freedom is again determined by applying the principle of minimum potential energy ($\partial\Pi/\partial\theta_{xz} = 0$). Once we have the energy as a function of u_z, the force-displacement curve is obtained by computing its derivative. The slope of the force-displacement curve gives the stiffness of the unit in both stable states.

Fig. 4.15 compare the force-displacement curves obtained experimentally, through FE simulations and via the semi-analytical model, in both stable states, and for three geometries : iso-stiffness, softening, stiffening. The good agreement between the experiments and the semi-analytical model, allows us to validate the latter.

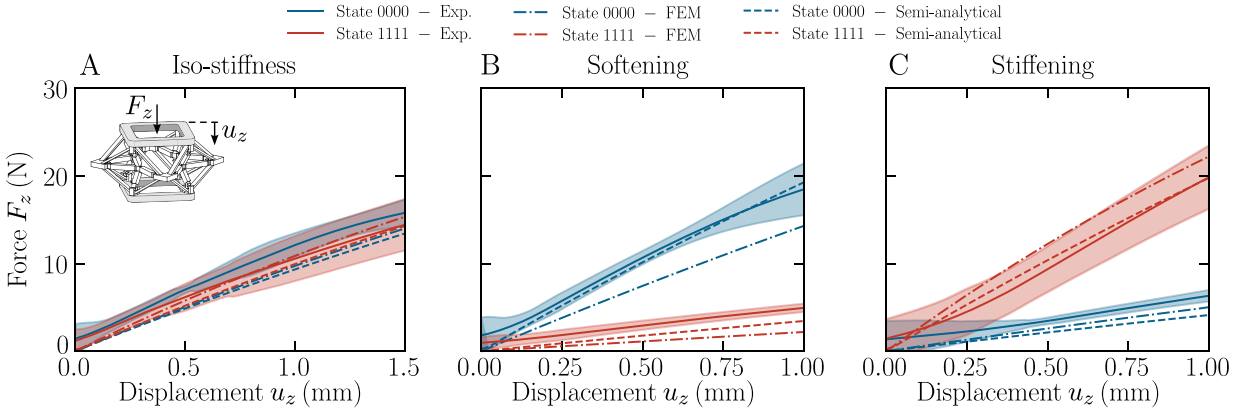

Figure 4.15 | **Comparison of the force-displacement curves obtained with semi-analytical model, FE analysis and experiments** The force-displacement curves correspond to the compression of **(A)** the iso-stiffness unit, **(B)** the softening unit and **(C)** the stiffening unit, in both stable states.

4.13.2 Limit cases

The softest configurations are obtained for the maximal value of θ_{0xz}, when the joints bear most of the load. We can model the unit by only considering the joints of the von Mises trusses in the $xz-$plane, represented as torsion springs (see Fig. 4.16A).

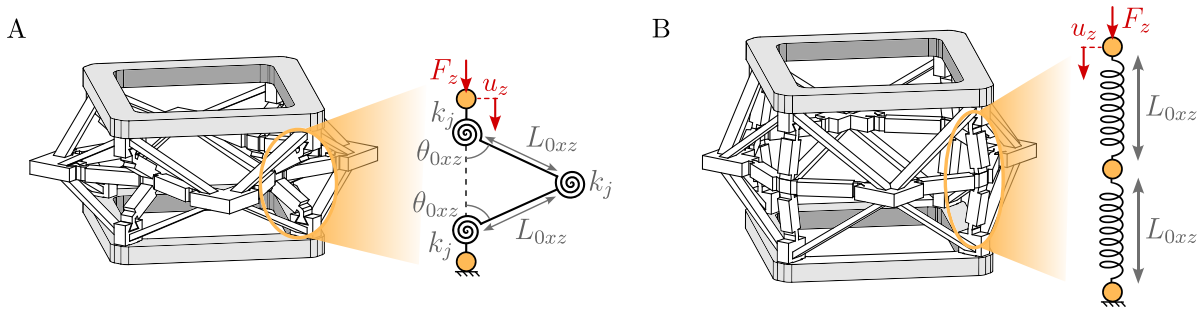

Figure 4.16 | **Limit cases (A)** The softest configurations are obtained when the value of θ_{0xz} is maximal, that is, when the joints support most of the load. **(B)** The stiffest configurations are obtained for $\theta_{0xz} = 0°$, when the vertical trusses support most of the load.

Based on the geometry, we can deduce a relation between the displacement u_z applied at the top of the unit, and the angle θ_{xz} :

$$\theta_{xz} = \arccos\left(\cos(\theta_{0xz}) - \frac{u_z}{2L_{0xz}}\right). \tag{4.18}$$

The reaction force of the unit is calculated as the derivative of the energy with respect to the control parameter u_z :

$$\Pi = 12k_j(\theta_{xz} - \theta_{0xz})^2, \tag{4.19}$$

$$F_z = \frac{d\Pi}{du_z} = 24k_j(\theta_{xz} - \theta_{0xz})\frac{d\theta_{xz}}{du_z}. \tag{4.20}$$

The stiffness of the unit is given by the initial slope of the force-displacement curve :

$$K_{min} = \frac{dF_z}{du_z}(u_z = 0) = \frac{6k_j}{(L_{0xz} + l_j)^2 \sin^2(\theta_{0xz})} = 1.4 \text{ N/mm}. \tag{4.21}$$

The stiffest configurations are obtained for the minimal value of θ_{0xz}, when the trusses in the $xz-$plane bear most of the load. We can model the unit by only considering the trusses in the $xz-$plane, represented as axial springs (see Fig. 4.16B). The compressive stiffness of the

unit is therefore :

$$K_{max} = 4\frac{E_0 A_{xz}}{2L_{0xz}} = 88,3 \text{ N/mm} \tag{4.22}$$

4.14 Supplementary information : Section S4. Applications

4.14.1 Modularity

The coupled von Mises trusses within each face can be substituted with a new geometry provided that several conditions ensuring geometric compatibility are met. If the initial geometry is characterized by $r_L, \theta_{0xy}, \theta_{0xz}$ and L_{0xz}, and the new geometry is defined by $r_L^{'}, \theta_{0xy}^{'}, \theta_{0xz}^{'}$ and $L_{0xz}^{'}$, then the conditions of compatibility are :

$$\begin{aligned}(L_{0xz} + L_j)\ \sin(\theta_{0xz}) - (r_L L_{0xz} + L_j)\ \sin(\theta_{0xy}) = \\ (L_{0xz}^{'} + L_j)\ \sin(\theta_{0xz}^{'}) - (r_L^{'} L_{0xz}^{'} + L_j)\ \sin(\theta_{0xy}^{'}),\end{aligned} \tag{4.23}$$

$$(r_L L_{0xz} + L_j)\ \cos(\theta_{0xy}) = (r_L^{'} L_{0xz}^{'} + L_j)\ \cos(\theta_{0xy}^{'}), \tag{4.24}$$

$$(L_{0xz} + L_j)\ \cos(\theta_{0xz}) = (L_{0xz}^{'} + L_j)\ \cos(\theta_{0xz}^{'}). \tag{4.25}$$

Equation (4.23) impose that Δ remains unchanged, equation (4.24) ensures that the width of the frame stays identical and equation (4.25) maintains the height of the frame.

4.14.2 Sandwich panel with morphing surface

This section explains the methodology used to select the units for constructing the saddle-shaped surface. We aim to identify two unit geometries: unit α with height H_0 in state 0000 and H_1 in state 1111, and unit β with height H_0' in state 0000 and H_1' in state 1111. These units are organized as shown in Fig. 4.17A to form the sandwich panel. Using our analytical model, we map the height variation that occurs when switching from state 0000 to state 1111 as a function of the parameters in our design space. Unit α is selected from the region where the analytical model indicates maximum deformation: $r_L = 1.6$, $\theta_{0xy} = 23°$, $\theta_{0xz} = 72°$ with $L_{0xz} = 10$ mm (see Fig. 4.17B). Once unit α's geometry is fixed, we determine unit β's geometry to meet two conditions: (1) the height of unit α in state 1111 must match the height of unit β in state 0000 for a continuous surface (i.e., $H_1 = H_0'$), and (2) the top and bottom parts of both units should be identical to allow interchangeability and achieve different shapes with the same sandwich panel. Based on the geometry of the unit, we find that this second condition translates into equation 4.26, which ensures that the diagonals of the top and bottom parts of both units α and β are identical :

$$r_L^\beta = \frac{\frac{L_{0xy}^\alpha \cos(\theta_{0xy}^\alpha)}{\tan(\pi/4)} - L_{0xy}^\alpha \sin(\theta_{0xy}^\alpha) + L_{0xz}^\alpha \sin(\theta_{0xz}^\alpha) - L_{0xz}^\beta \sin(\theta_{0xz}^\beta)}{\frac{L_{0xz}^\beta \cos(\theta_{0xy}^\beta)}{\tan(\pi/4)} - L_{0xz}^\beta \sin(\theta_{0xy}^\beta)} \tag{4.26}$$

We set the length of the von Mises truss in the $xz-$plane, L_{0xz}, and the angle θ_{0xz} to satisfy condition (1), ensuring that θ_{0xz} is neither too large for easy actuation nor too small for significant height variation. Two parameters remain undetermined: r_L and θ_{0xy}. Using the analytical model, we map the deformation in the corresponding 2D design space (see Fig. 4.17C). We also indicate the configurations with the same top and bottom parts as unit α with a dotted line (corresponding to the equation above). Unit β is chosen from this line to meet condition (2) and from the area of maximum deformation $r_L = 1.14$, $\theta_{0xy} = 28°$, $\theta_{0xz} = 58°$ with $L_{0xz} = 14$ mm.

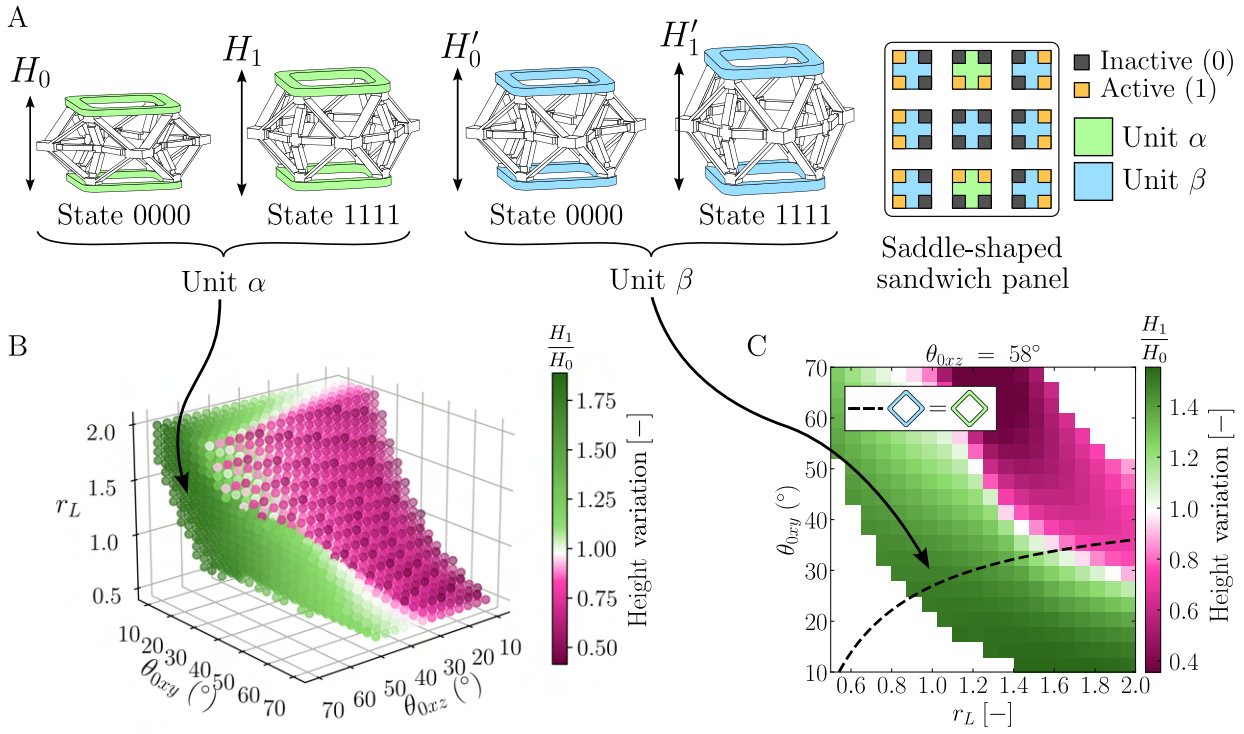

Figure 4.17 | **Selection and configuration of units for the saddle-shaped surface**

CHAPTER 5 CONCLUSION

5.1 Summary of contributions

A multistable mechanical metamaterial was introduced, integrating three key properties : stiffness tunability, shape morphing capabilities, and modularity. The core mechanism leveraged to achieve stiffness variation and shape transformation is the geometric frustration arising from two coupled von Mises trusses. Finite element and semi-analytical models were developed to investigate the influence of geometry on the mechanical properties, revealing three distinct cases : (1) no stiffness and height variation, (2) decreasing stiffness and height and (3) increasing stiffness and height. A notable finding of this study is that a simple geometric parameter, denoted as Δ and representing the distance between the ends of the two coupled von Mises trusses, determines the specific case in which a unit cell geometry falls. Several applications were developed to showcase the full potential of the proposed metamaterials. First, we demonstrated the capacity to change the stiffness variation of a unit post-fabrication using modularity, reducing the stiffness variation of a unit by around a factor of two. This was followed by the creation of a sandwich panel with tunable compressive and bending stiffness, achieving stiffness ratios of 1.56 and 2.12 respectively. Lastly, the shape morphing abilities of the units were utilized to build a sandwich panel with a morphing surface.

5.2 Limitations and future research

The work presented in this Master's thesis highlights several limitations that could be addressed in future research. First, manual actuation is used to transition between the stable states, which significantly narrows the range of possible applications. Practical engineering uses would require remote and automated actuation. Several approaches could be explored, such as integrating materials responsive to external stimuli like temperature (Mueller et al., 2022; Niknam et al., 2022), magnetic fields (Jackson et al., 2018; Chen et al., 2021; Ramachandran et al., 2016) or light (Shankar et al., 2013). Pneumatic actuation, which has been widely applied in multistable structures, also presents a promising direction (Melancon et al., 2022, 2021; Gorissen et al., 2020; Rahman et al., 2023). A system utilizing shape memory alloys has also been employed to actuate a von Mises truss (Barbarino et al., 2013), though adaptation is necessary to suit the smaller scale required for this work.

While using FFF with PLA and TPU successfully achieved the required mechanical proper-

ties, the fabrication method could be improved in two significant ways: reducing the number of parts to assemble and decreasing the scale of the unit. Recent advancements in commercial FFF printers now allow for the use of more than two materials in one print. Adopting these advanced multimaterial 3D printing techniques could effectively address these challenges.

Finally, the curvature achievable by the morphing surface of the sandwich panel is constrained due to the stretching of the polymer sheet. The precision of the curvature is also limited by the number of units used to build the sandwich panel. In order overcome these limitations, a softer material could be used to enable larger deformation. Another approach would be to replace the continuous surface by overlapping scales that can slide relative to one another (K. Liu et al., 2021).

REFERENCES

Abbasi, Arefeh, Tian Chen, Bastien F.G. Aymon, and Pedro M. Reis. "Leveraging the Snap Buckling of Bistable Magnetic Shells to Design a Refreshable Braille Dot". In: *Advanced Materials Technologies* 9.3 (Feb. 2024), p. 2301344. ISSN: 2365-709X, 2365-709X. DOI: 10.1002/admt.202301344. URL: https://onlinelibrary.wiley.com/doi/10.1002/admt.202301344 (visited on 08/15/2024).

Barbarino, Silvestro, Farhan S. Gandhi, and Rodolphe Visdeloup. "A Bi-Stable von-Mises Truss for Morphing Applications Actuated Using Shape Memory Alloys". In: *Volume 1: Development and Characterization of Multifunctional Materials; Modeling, Simulation and Control of Adaptive Systems; Integrated System Design and Implementation*. ASME 2013 Conference on Smart Materials, Adaptive Structures and Intelligent Systems. Snowbird, Utah, USA: American Society of Mechanical Engineers, Sept. 16, 2013, V001T01A004. ISBN: 9780791856031. DOI: 10.1115/SMASIS2013-3062. URL: https://asmedigitalcollection.asme.org/SMASIS/proceedings/SMASIS2013/56031/Snowbird,%20Utah,%20USA/283997 (visited on 07/25/2024).

Bertoldi, Katia, Vincenzo Vitelli, Johan Christensen, and Martin Van Hecke. "Flexible mechanical metamaterials". In: *Nature Reviews Materials* 2.11 (Oct. 17, 2017), p. 17066. ISSN: 2058-8437. DOI: 10.1038/natrevmats.2017.66. URL: https://www.nature.com/articles/natrevmats201766 (visited on 05/29/2024).

Bobbert, F.S.L., S. Janbaz, T. Van Manen, Y. Li, and A.A. Zadpoor. "Russian doll deployable meta-implants: Fusion of kirigami, origami, and multi-stability". In: *Materials & Design* 191 (June 2020), p. 108624. ISSN: 02641275. DOI: 10.1016/j.matdes.2020.108624. URL: https://linkinghub.elsevier.com/retrieve/pii/S0264127520301581 (visited on 08/06/2024).

Chen, Tian, Mark Pauly, and Pedro M. Reis. "A reprogrammable mechanical metamaterial with stable memory". In: *Nature* 589.7842 (Jan. 21, 2021), pp. 386–390. ISSN: 0028-0836, 1476-4687. DOI: 10.1038/s41586-020-03123-5. URL: https://www.nature.com/articles/s41586-020-03123-5 (visited on 07/16/2024).

Chen, Tian and Kristina Shea. "Computational design of multi-stable, reconfigurable surfaces". In: *Materials & Design* 205 (July 2021), p. 109688. ISSN: 02641275. DOI: 10.1016/j.matdes.2021.109688. URL: https://linkinghub.elsevier.com/retrieve/pii/S0264127521002409 (visited on 05/01/2024).

Chi, Yinding, Yanbin Li, Yao Zhao, Yaoye Hong, Yichao Tang, and Jie Yin. "Bistable and Multistable Actuators for Soft Robots: Structures, Materials, and Functionalities". In:

Advanced Materials 34.19 (May 2022), p. 2110384. ISSN: 0935-9648, 1521-4095. DOI: 10.1002/adma.202110384. URL: https://onlinelibrary.wiley.com/doi/10.1002/adma.202110384 (visited on 05/01/2024).

Coulais, Corentin, Eial Teomy, Koen De Reus, Yair Shokef, and Martin Van Hecke. "Combinatorial design of textured mechanical metamaterials". In: *Nature* 535.7613 (July 2016), pp. 529–532. ISSN: 0028-0836, 1476-4687. DOI: 10.1038/nature18960. URL: https://www.nature.com/articles/nature18960 (visited on 05/01/2024).

De Jong, Pier H., Y. Salvatori, F. Libonati, Mohammad J. Mirzaali, and Amir A. Zadpoor. "Shape-locking in architected materials through 3D printed magnetically activated joints". en. In: *Materials & Design* 235 (Nov. 2023), p. 112427. ISSN: 02641275. DOI: 10.1016/j.matdes.2023.112427. URL: https://linkinghub.elsevier.com/retrieve/pii/S0264127523008420 (visited on 08/27/2024).

Fang, Hongbin, Shih-Cheng A. Chu, Yutong Xia, and Kon-Well Wang. "Programmable Self-Locking Origami Mechanical Metamaterials". In: *Advanced Materials* 30.15 (Apr. 2018), p. 1706311. ISSN: 0935-9648, 1521-4095. DOI: 10.1002/adma.201706311. URL: https://onlinelibrary.wiley.com/doi/10.1002/adma.201706311 (visited on 05/01/2024).

Forterre, Yoël, Jan M. Skotheim, Jacques Dumais, and L. Mahadevan. "How the Venus flytrap snaps". In: *Nature* 433.7024 (Jan. 2005), pp. 421–425. ISSN: 0028-0836, 1476-4687. DOI: 10.1038/nature03185. URL: https://www.nature.com/articles/nature03185 (visited on 08/15/2024).

Gorissen, Benjamin, David Melancon, Nikolaos Vasios, Mehdi Torbati, and Katia Bertoldi. "Inflatable soft jumper inspired by shell snapping". In: *Science Robotics* 5.42 (May 13, 2020), eabb1967. ISSN: 2470-9476. DOI: 10.1126/scirobotics.abb1967. URL: https://www.science.org/doi/10.1126/scirobotics.abb1967 (visited on 07/16/2024).

Guseinov, Ruslan, Connor McMahan, Jesús Pérez, Chiara Daraio, and Bernd Bickel. "Programming temporal morphing of self-actuated shells". en. In: *Nature Communications* 11.1 (Jan. 2020), p. 237. ISSN: 2041-1723. DOI: 10.1038/s41467-019-14015-2. URL: https://www.nature.com/articles/s41467-019-14015-2 (visited on 08/27/2024).

Haghpanah, Babak, Ladan Salari-Sharif, Peyman Pourrajab, Jonathan Hopkins, and Lorenzo Valdevit. "Multistable Shape-Reconfigurable Architected Materials". In: *Advanced Materials* 28.36 (Sept. 2016), pp. 7915–7920. ISSN: 0935-9648, 1521-4095. DOI: 10.1002/adma.201601650. URL: https://onlinelibrary.wiley.com/doi/10.1002/adma.201601650 (visited on 09/22/2022).

Hwang, Dohgyu, Edward J. Barron, A. B. M. Tahidul Haque, and Michael D. Bartlett. "Shape morphing mechanical metamaterials through reversible plasticity". In: *Science Robotics* 7.63 (Feb. 23, 2022), eabg2171. ISSN: 2470-9476. DOI: 10.1126/scirobotics.abg2171.

URL: https://www.science.org/doi/10.1126/scirobotics.abg2171 (visited on 07/25/2024).

Jackson, Julie A., Mark C. Messner, Nikola A. Dudukovic, William L. Smith, Logan Bekker, Bryan Moran, Alexandra M. Golobic, Andrew J. Pascall, Eric B. Duoss, Kenneth J. Loh, and Christopher M. Spadaccini. "Field responsive mechanical metamaterials". In: *Science Advances* 4.12 (Dec. 7, 2018), eaau6419. ISSN: 2375-2548. DOI: 10.1126/sciadv.aau6419. URL: https://www.science.org/doi/10.1126/sciadv.aau6419 (visited on 07/16/2024).

Jensen, B. D., L. L. Howell, and L. G. Salmon. "Design of Two-Link, In-Plane, Bistable Compliant Micro-Mechanisms". In: *Journal of Mechanical Design* 121.3 (Sept. 1, 1999), pp. 416–423. ISSN: 1050-0472, 1528-9001. DOI: 10.1115/1.2829477. URL: https://asmedigitalcollection.asme.org/mechanicaldesign/article/121/3/416/417937/Design-of-TwoLink-InPlane-Bistable-Compliant (visited on 08/15/2024).

Jiang, Caigui, Florian Rist, Hui Wang, Johannes Wallner, and Helmut Pottmann. "Shape-morphing mechanical metamaterials". In: *Computer-Aided Design* 143 (Feb. 2022), p. 103146. ISSN: 00104485. DOI: 10.1016/j.cad.2021.103146. URL: https://linkinghub.elsevier.com/retrieve/pii/S0010448521001573 (visited on 07/23/2024).

Jiang, Yijie, Lucia M. Korpas, and Jordan R. Raney. "Bifurcation-based embodied logic and autonomous actuation". In: *Nature Communications* 10.1 (Jan. 10, 2019), p. 128. ISSN: 2041-1723. DOI: 10.1038/s41467-018-08055-3. URL: https://www.nature.com/articles/s41467-018-08055-3 (visited on 08/05/2024).

Jiao, Pengcheng, Jochen Mueller, Jordan R. Raney, Xiaoyu Zheng, and Amir H. Alavi. "Mechanical metamaterials and beyond". en. In: *Nature Communications* 14.1 (Sept. 2023), p. 6004. ISSN: 2041-1723. DOI: 10.1038/s41467-023-41679-8. URL: https://www.nature.com/articles/s41467-023-41679-8 (visited on 08/27/2024).

Li, Yanbin, Antonio Di Lallo, Junxi Zhu, Yinding Chi, Hao Su, and Jie Yin. "Adaptive hierarchical origami-based metastructures". In: *Nature Communications* 15.1 (July 26, 2024), p. 6247. ISSN: 2041-1723. DOI: 10.1038/s41467-024-50497-5. URL: https://www.nature.com/articles/s41467-024-50497-5 (visited on 08/13/2024).

Li, Yanbin, Qiuting Zhang, Yaoye Hong, and Jie Yin. "3D Transformable Modular Kirigami Based Programmable Metamaterials". In: *Advanced Functional Materials* 31.43 (Oct. 2021), p. 2105641. ISSN: 1616-301X, 1616-3028. DOI: 10.1002/adfm.202105641. URL: https://onlinelibrary.wiley.com/doi/10.1002/adfm.202105641 (visited on 04/26/2024).

Librandi, Gabriele, Eleonora Tubaldi, and Katia Bertoldi. "Programming nonreciprocity and reversibility in multistable mechanical metamaterials". en. In: *Nature Communications*

12.1 (June 2021), p. 3454. ISSN: 2041-1723. DOI: 10.1038/s41467-021-23690-z. URL: https://www.nature.com/articles/s41467-021-23690-z (visited on 08/27/2024).

Liu, Ke, Felix Hacker, and Chiara Daraio. "Robotic surfaces with reversible, spatiotemporal control for shape morphing and object manipulation". In: *Science Robotics* 6.53 (Apr. 28, 2021), eabf5116. ISSN: 2470-9476. DOI: 10.1126/scirobotics.abf5116. URL: https://www.science.org/doi/10.1126/scirobotics.abf5116 (visited on 07/31/2024).

Liu, Qingjiang, Haitao Ye, Jianxiang Cheng, Honggeng Li, Xiangnan He, Bingcong Jian, and Qi Ge. "Stiffness-Tunable Origami Structures via Multimaterial Three-Dimensional Printing". In: *Acta Mechanica Solida Sinica* 36.4 (Aug. 2023), pp. 582–593. ISSN: 0894-9166, 1860-2134. DOI: 10.1007/s10338-023-00403-1. URL: https://link.springer.com/10.1007/s10338-023-00403-1 (visited on 05/01/2024).

Mao, Jia-Jia, Shuai Wang, Wei Tan, and Mingchao Liu. "Modular multistable metamaterials with reprogrammable mechanical properties". In: *Engineering Structures* 272 (Dec. 2022), p. 114976. ISSN: 01410296. DOI: 10.1016/j.engstruct.2022.114976. URL: https://linkinghub.elsevier.com/retrieve/pii/S0141029622010525 (visited on 04/26/2024).

Meeussen, A. S. and M. Van Hecke. "Multistable sheets with rewritable patterns for switchable shape-morphing". In: *Nature* 621.7979 (Sept. 21, 2023), pp. 516–520. ISSN: 0028-0836, 1476-4687. DOI: 10.1038/s41586-023-06353-5. URL: https://www.nature.com/articles/s41586-023-06353-5 (visited on 05/01/2024).

Melancon, David, Antonio Elia Forte, Leon M. Kamp, Benjamin Gorissen, and Katia Bertoldi. "Inflatable Origami: Multimodal Deformation via Multistability". In: *Advanced Functional Materials* 32.35 (Aug. 2022), p. 2201891. ISSN: 1616-301X, 1616-3028. DOI: 10.1002/adfm.202201891. URL: https://onlinelibrary.wiley.com/doi/10.1002/adfm.202201891 (visited on 07/16/2024).

Melancon, David, Benjamin Gorissen, Carlos J. García-Mora, Chuck Hoberman, and Katia Bertoldi. "Multistable inflatable origami structures at the metre scale". In: *Nature* 592.7855 (Apr. 22, 2021), pp. 545–550. ISSN: 0028-0836, 1476-4687. DOI: 10.1038/s41586-021-03407-4. URL: https://www.nature.com/articles/s41586-021-03407-4 (visited on 07/19/2024).

Mintchev, Stefano, Jun Shintake, and Dario Floreano. "Bioinspired dual-stiffness origami". In: *Science Robotics* 3.20 (July 25, 2018), eaau0275. ISSN: 2470-9476. DOI: 10.1126/scirobotics.aau0275. URL: https://www.science.org/doi/10.1126/scirobotics.aau0275 (visited on 06/04/2024).

Mofatteh, Hossein, Benyamin Shahryari, Armin Mirabolghasemi, Alireza Seyedkanani, Razieh Shirzadkhani, Gilles Desharnais, and Abdolhamid Akbarzadeh. "Programming Mul-

tistable Metamaterials to Discover Latent Functionalities". en. In: *Advanced Science* 9.33 (Nov. 2022), p. 2202883. ISSN: 2198-3844, 2198-3844. DOI: 10.1002/advs.202202883. URL: https://onlinelibrary.wiley.com/doi/10.1002/advs.202202883 (visited on 08/27/2024).

Mousanezhad, Davood, Soroush Kamrava, and Ashkan Vaziri. "Origami-based Building Blocks for Modular Construction of Foldable Structures". In: *Scientific Reports* 7.1 (Nov. 1, 2017), p. 14792. ISSN: 2045-2322. DOI: 10.1038/s41598-017-13654-z. URL: https://www.nature.com/articles/s41598-017-13654-z (visited on 08/06/2024).

Mueller, Jochen, Jennifer A. Lewis, and Katia Bertoldi. "Architected Multimaterial Lattices with Thermally Programmable Mechanical Response". In: *Advanced Functional Materials* 32.1 (Jan. 2022), p. 2105128. ISSN: 1616-301X, 1616-3028. DOI: 10.1002/adfm.202105128. URL: https://onlinelibrary.wiley.com/doi/10.1002/adfm.202105128 (visited on 07/16/2024).

Niknam, Hamed, Abdolhamid Akbarzadeh, Daniel Therriault, and Sampada Bodkhe. "Tunable thermally bistable multi-material structure". In: *Applied Materials Today* 28 (Aug. 2022), p. 101529. ISSN: 23529407. DOI: 10.1016/j.apmt.2022.101529. URL: https://linkinghub.elsevier.com/retrieve/pii/S2352940722001640 (visited on 07/16/2024).

Overvelde, J. T. B., S. Shan, and K. Bertoldi. "Compaction Through Buckling in 2D Periodic, Soft and Porous Structures: Effect of Pore Shape". In: *Advanced Materials* 24.17 (May 2, 2012), pp. 2337–2342. ISSN: 0935-9648, 1521-4095. DOI: 10.1002/adma.201104395. URL: https://onlinelibrary.wiley.com/doi/10.1002/adma.201104395 (visited on 08/02/2024).

Overvelde, Johannes T. B., Tamara Kloek, Jonas J. A. D'haen, and Katia Bertoldi. "Amplifying the response of soft actuators by harnessing snap-through instabilities". In: *Proceedings of the National Academy of Sciences* 112.35 (Sept. 2015), pp. 10863–10868. ISSN: 0027-8424, 1091-6490. DOI: 10.1073/pnas.1504947112. URL: https://pnas.org/doi/full/10.1073/pnas.1504947112 (visited on 08/15/2024).

Overvelde, Johannes T.B., Twan A. De Jong, Yanina Shevchenko, Sergio A. Becerra, George M. Whitesides, James C. Weaver, Chuck Hoberman, and Katia Bertoldi. "A three-dimensional actuated origami-inspired transformable metamaterial with multiple degrees of freedom". In: *Nature Communications* 7.1 (Mar. 11, 2016), p. 10929. ISSN: 2041-1723. DOI: 10.1038/ncomms10929. URL: https://www.nature.com/articles/ncomms10929 (visited on 05/01/2024).

Rafsanjani, Ahmad, Abdolhamid Akbarzadeh, and Damiano Pasini. "Snapping Mechanical Metamaterials under Tension". In: *Advanced Materials* 27.39 (Oct. 2015), pp. 5931–5935.

ISSN: 09359648. DOI: 10.1002/adma.201502809. URL: https://onlinelibrary.wiley.com/doi/10.1002/adma.201502809 (visited on 09/18/2022).

Rahman, Shakurur, Lei Wu, Asma El Elmi, and Damiano Pasini. "Zero-Power Shape Retention in Soft Pneumatic Actuators with Extensional and Bending Multistability". In: *Advanced Functional Materials* 33.49 (Dec. 2023), p. 2304151. ISSN: 1616-301X, 1616-3028. DOI: 10.1002/adfm.202304151. URL: https://onlinelibrary.wiley.com/doi/10.1002/adfm.202304151 (visited on 07/16/2024).

Ramachandran, Vivek, Michael D. Bartlett, James Wissman, and Carmel Majidi. "Elastic instabilities of a ferroelastomer beam for soft reconfigurable electronics". In: *Extreme Mechanics Letters* 9 (Dec. 2016), pp. 282–290. ISSN: 23524316. DOI: 10.1016/j.eml.2016.08.007. URL: https://linkinghub.elsevier.com/retrieve/pii/S2352431615300432 (visited on 07/16/2024).

Raviv, Dan, Wei Zhao, Carrie McKnelly, Athina Papadopoulou, Achuta Kadambi, Boxin Shi, Shai Hirsch, Daniel Dikovsky, Michael Zyracki, Carlos Olguin, Ramesh Raskar, and Skylar Tibbits. "Active Printed Materials for Complex Self-Evolving Deformations". In: *Scientific Reports* 4.1 (Dec. 18, 2014), p. 7422. ISSN: 2045-2322. DOI: 10.1038/srep07422. URL: https://www.nature.com/articles/srep07422 (visited on 07/25/2024).

Restrepo, David, Nilesh D. Mankame, and Pablo D. Zavattieri. "Phase transforming cellular materials". In: *Extreme Mechanics Letters* 4 (Sept. 2015), pp. 52–60. ISSN: 23524316. DOI: 10.1016/j.eml.2015.08.001. URL: https://linkinghub.elsevier.com/retrieve/pii/S2352431615000929 (visited on 08/05/2024).

Risso, Giada, Max Kudisch, Paolo Ermanni, and Chiara Daraio. "Tuning the Properties of Multi-Stable Structures Post-Fabrication Via the Two-Way Shape Memory Polymer Effect". In: *Advanced Science* 11.21 (June 2024), p. 2308903. ISSN: 2198-3844, 2198-3844. DOI: 10.1002/advs.202308903. URL: https://onlinelibrary.wiley.com/doi/10.1002/advs.202308903 (visited on 08/13/2024).

Schaedler, T. A., A. J. Jacobsen, A. Torrents, A. E. Sorensen, J. Lian, J. R. Greer, L. Valdevit, and W. B. Carter. "Ultralight Metallic Microlattices". In: *Science* 334.6058 (Nov. 18, 2011), pp. 962–965. ISSN: 0036-8075, 1095-9203. DOI: 10.1126/science.1211649. URL: https://www.science.org/doi/10.1126/science.1211649 (visited on 08/05/2024).

Shankar, M. Ravi, Matthew L. Smith, Vincent P. Tondiglia, Kyung Min Lee, Michael E. McConney, David H. Wang, Loon-Seng Tan, and Timothy J. White. "Contactless, photoinitiated snap-through in azobenzene-functionalized polymers". In: *Proceedings of the National Academy of Sciences* 110.47 (Nov. 19, 2013), pp. 18792–18797. ISSN: 0027-8424, 1091-6490. DOI: 10.1073/pnas.1313195110. URL: https://pnas.org/doi/full/10.1073/pnas.1313195110 (visited on 07/16/2024).

Shi, Jiahao, Hossein Mofatteh, Armin Mirabolghasemi, Gilles Desharnais, and Abdolhamid Akbarzadeh. "Programmable Multistable Perforated Shellular". In: *Advanced Materials* 33.42 (Oct. 2021), p. 2102423. ISSN: 0935-9648, 1521-4095. DOI: 10.1002/adma.202102423. URL: https://onlinelibrary.wiley.com/doi/10.1002/adma.202102423 (visited on 08/06/2024).

Siéfert, Emmanuel, Etienne Reyssat, José Bico, and Benoît Roman. "Programming curvilinear paths of flat inflatables". In: *Proceedings of the National Academy of Sciences* 116.34 (Aug. 20, 2019), pp. 16692–16696. ISSN: 0027-8424, 1091-6490. DOI: 10.1073/pnas.1904544116. URL: https://pnas.org/doi/full/10.1073/pnas.1904544116 (visited on 07/26/2024).

Silverberg, Jesse L., Arthur A. Evans, Lauren McLeod, Ryan C. Hayward, Thomas Hull, Christian D. Santangelo, and Itai Cohen. "Using origami design principles to fold reprogrammable mechanical metamaterials". In: *Science* 345.6197 (Aug. 8, 2014), pp. 647–650. ISSN: 0036-8075, 1095-9203. DOI: 10.1126/science.1252876. URL: https://www.science.org/doi/10.1126/science.1252876 (visited on 06/04/2024).

Sonego, Monique, Márcia Elisa Soares Echeveste, and Henrique Galvan Debarba. "The role of modularity in sustainable design: A systematic review". In: *Journal of Cleaner Production* 176 (Mar. 2018), pp. 196–209. ISSN: 09596526. DOI: 10.1016/j.jclepro.2017.12.106. URL: https://linkinghub.elsevier.com/retrieve/pii/S0959652617330561 (visited on 08/07/2024).

Tahidul Haque, A. B. M., Samuele Ferracin, and Jordan R. Raney. "Reprogrammable Mechanics via Individually Switchable Bistable Unit Cells in a Prestrained Chiral Metamaterial". In: *Advanced Materials Technologies* (May 30, 2024), p. 2400474. ISSN: 2365-709X, 2365-709X. DOI: 10.1002/admt.202400474. URL: https://onlinelibrary.wiley.com/doi/10.1002/admt.202400474 (visited on 06/06/2024).

Tang, Yichao, Yinding Chi, Jiefeng Sun, Tzu-Hao Huang, Omid H. Maghsoudi, Andrew Spence, Jianguo Zhao, Hao Su, and Jie Yin. "Leveraging elastic instabilities for amplified performance: Spine-inspired high-speed and high-force soft robots". In: *Science Advances* 6.19 (May 8, 2020), eaaz6912. ISSN: 2375-2548. DOI: 10.1126/sciadv.aaz6912. URL: https://www.science.org/doi/10.1126/sciadv.aaz6912 (visited on 05/01/2024).

Terwagne, Denis, Miha Brojan, and Pedro M. Reis. "Smart Morphable Surfaces for Aerodynamic Drag Control". In: *Advanced Materials* 26.38 (Oct. 2014), pp. 6608–6611. ISSN: 0935-9648, 1521-4095. DOI: 10.1002/adma.201401403. URL: https://onlinelibrary.wiley.com/doi/10.1002/adma.201401403 (visited on 05/01/2024).

Tondi, G., A. Pizzi, and R. Olives. "Natural tannin-based rigid foams as insulation for doors and wall panels". In: *Maderas. Ciencia y tecnología* 10.3 (2008), pp. 219–227. ISSN: 0718-

221X. DOI: 10.4067/S0718-221X2008000300005. URL: http://www.scielo.cl/scielo.php?script=sci_abstract&pid=S0718-221X2008000300005&lng=en&nrm=iso&tlng=en (visited on 08/05/2024).

Udani, Janav P. and Andres F. Arrieta. "Programmable mechanical metastructures from locally bistable domes". In: *Extreme Mechanics Letters* 42 (Jan. 2021), p. 101081. ISSN: 23524316. DOI: 10.1016/j.eml.2020.101081. URL: https://linkinghub.elsevier.com/retrieve/pii/S2352431620302674 (visited on 05/01/2024).

Vyatskikh, Andrey, Stéphane Delalande, Akira Kudo, Xuan Zhang, Carlos M. Portela, and Julia R. Greer. "Additive manufacturing of 3D nano-architected metals". In: *Nature Communications* 9.1 (Dec. 2018), p. 593. ISSN: 2041-1723. DOI: 10.1038/s41467-018-03071-9. URL: http://www.nature.com/articles/s41467-018-03071-9 (visited on 09/22/2022).

Wang, Qiming, Julie A. Jackson, Qi Ge, Jonathan B. Hopkins, Christopher M. Spadaccini, and Nicholas X. Fang. "Lightweight Mechanical Metamaterials with Tunable Negative Thermal Expansion". In: *Physical Review Letters* 117.17 (Oct. 21, 2016), p. 175901. DOI: 10.1103/PhysRevLett.117.175901. URL: https://link.aps.org/doi/10.1103/PhysRevLett.117.175901 (visited on 08/02/2024).

Wang, Xiaolei, Haibo Qu, Xiao Li, Yili Kuang, Haoqian Wang, and Sheng Guo. "Multi-triangles cylindrical origami and inspired metamaterials with tunable stiffness and stretchable robotic arm". In: *PNAS Nexus* (Mar. 23, 2023), pgad098. ISSN: 2752-6542. DOI: 10.1093/pnasnexus/pgad098. URL: https://academic.oup.com/pnasnexus/advance-article/doi/10.1093/pnasnexus/pgad098/7084473 (visited on 03/28/2023).

Wang, Yifan, Liuchi Li, Douglas Hofmann, José E. Andrade, and Chiara Daraio. "Structured fabrics with tunable mechanical properties". In: *Nature* 596.7871 (Aug. 12, 2021), pp. 238–243. ISSN: 0028-0836, 1476-4687. DOI: 10.1038/s41586-021-03698-7. URL: https://www.nature.com/articles/s41586-021-03698-7 (visited on 06/04/2024).

Wo, Zhongyuan and Evgueni T. Filipov. "Stiffening multi-stable origami tubes by outward popping of creases". In: *Extreme Mechanics Letters* 58 (Jan. 2023), p. 101941. ISSN: 23524316. DOI: 10.1016/j.eml.2022.101941. URL: https://linkinghub.elsevier.com/retrieve/pii/S2352431622002176 (visited on 05/01/2024).

Wu, Lei and Damiano Pasini. "Topological Transformation with Emerging Zero Modes in Multistable Metamaterials for Reprogrammable Flexural Stiffness". In: *Physical Review Applied* 19.6 (June 22, 2023), p. L061001. ISSN: 2331-7019. DOI: 10.1103/PhysRevApplied.19.L061001. URL: https://link.aps.org/doi/10.1103/PhysRevApplied.19.L061001 (visited on 05/01/2024).

Wu, Lei and Damiano Pasini. "Zero modes activation to reconcile floppiness, rigidity, and multistability into an all-in-one class of reprogrammable metamaterials". In: *Nature Communications* 15.1 (Apr. 10, 2024), p. 3087. ISSN: 2041-1723. DOI: 10.1038/s41467-024-47180-0. URL: https://www.nature.com/articles/s41467-024-47180-0 (visited on 06/04/2024).

Wu, Yi, Ying Han, Zhuxuan Wei, Yu Xie, Jun Yin, and Jin Qian. "4D Printing of Chiral Mechanical Metamaterials with Modular Programmability using Shape Memory Polymer". In: *Advanced Functional Materials* 33.52 (Dec. 2023), p. 2306442. ISSN: 1616-301X, 1616-3028. DOI: 10.1002/adfm.202306442. URL: https://onlinelibrary.wiley.com/doi/10.1002/adfm.202306442 (visited on 05/01/2024).

Yang, Yi, Marcelo A. Dias, and Douglas P. Holmes. "Multistable kirigami for tunable architected materials". In: *Physical Review Materials* 2.11 (Nov. 20, 2018), p. 110601. ISSN: 2475-9953. DOI: 10.1103/PhysRevMaterials.2.110601. URL: https://link.aps.org/doi/10.1103/PhysRevMaterials.2.110601 (visited on 05/01/2024).

Zadpoor, Amir A. "Mechanical meta-materials". en. In: *Materials Horizons* 3.5 (2016), pp. 371–381. ISSN: 2051-6347, 2051-6355. DOI: 10.1039/C6MH00065G. URL: https://xlink.rsc.org/?DOI=C6MH00065G (visited on 08/27/2024).

Zhai, Zirui, Yong Wang, and Hanqing Jiang. "Origami-inspired, on-demand deployable and collapsible mechanical metamaterials with tunable stiffness". In: *Proceedings of the National Academy of Sciences* 115.9 (Feb. 27, 2018), pp. 2032–2037. ISSN: 0027-8424, 1091-6490. DOI: 10.1073/pnas.1720171115. URL: https://pnas.org/doi/full/10.1073/pnas.1720171115 (visited on 05/01/2024).

Zhai, Zirui, Yong Wang, Ken Lin, Lingling Wu, and Hanqing Jiang. "In situ stiffness manipulation using elegant curved origami". In: *Science Advances* 6.47 (Nov. 20, 2020), eabe2000. ISSN: 2375-2548. DOI: 10.1126/sciadv.abe2000. URL: https://www.science.org/doi/10.1126/sciadv.abe2000 (visited on 05/01/2024).

Zhang, Hang, Jun Wu, Daining Fang, and Yihui Zhang. "Hierarchical mechanical metamaterials built with scalable tristable elements for ternary logic operation and amplitude modulation". In: *Science Advances* 7.9 (Feb. 26, 2021), eabf1966. ISSN: 2375-2548. DOI: 10.1126/sciadv.abf1966. URL: https://www.science.org/doi/10.1126/sciadv.abf1966 (visited on 08/06/2024).

Zhang, Yong, Marcel Tichem, and Fred Van Keulen. "Concept and design of a metastructure-based multi-stable surface". In: *Extreme Mechanics Letters* 51 (Feb. 2022), p. 101553. ISSN: 23524316. DOI: 10.1016/j.eml.2021.101553. URL: https://linkinghub.elsevier.com/retrieve/pii/S2352431621002200 (visited on 05/01/2024).

Zheng, Xiaoyu, Howon Lee, Todd H. Weisgraber, Maxim Shusteff, Joshua DeOtte, Eric B. Duoss, Joshua D. Kuntz, Monika M. Biener, Qi Ge, Julie A. Jackson, Sergei O. Kucheyev, Nicholas X. Fang, and Christopher M. Spadaccini. "Ultralight, ultrastiff mechanical metamaterials". In: *Science* 344.6190 (June 20, 2014), pp. 1373–1377. ISSN: 0036-8075, 1095-9203. DOI: 10.1126/science.1252291. URL: https://www.science.org/doi/10.1126/science.1252291 (visited on 08/02/2024).

Zhong, Q., J. Zhu, F. E. Fish, S. J. Kerr, A. M. Downs, H. Bart-Smith, and D. B. Quinn. "Tunable stiffness enables fast and efficient swimming in fish-like robots". In: *Science Robotics* 6.57 (Aug. 11, 2021), eabe4088. ISSN: 2470-9476. DOI: 10.1126/scirobotics.abe4088. URL: https://www.science.org/doi/10.1126/scirobotics.abe4088 (visited on 06/04/2024).

Zhou, Xueli, Luquan Ren, Zhengyi Song, Guiwei Li, Jifeng Zhang, Bingqian Li, Qian Wu, Wangxuan Li, Lei Ren, and Qingping Liu. "Advances in 3D/4D printing of mechanical metamaterials: From manufacturing to applications". In: *Composites Part B: Engineering* 254 (Apr. 2023), p. 110585. ISSN: 13598368. DOI: 10.1016/j.compositesb.2023.110585. URL: https://linkinghub.elsevier.com/retrieve/pii/S1359836823000884 (visited on 07/16/2024).

Zhu, Yi and Evgueni T. Filipov. "Large-scale modular and uniformly thick origami-inspired adaptable and load-carrying structures". In: *Nature Communications* 15.1 (Mar. 15, 2024), p. 2353. ISSN: 2041-1723. DOI: 10.1038/s41467-024-46667-0. URL: https://www.nature.com/articles/s41467-024-46667-0 (visited on 08/13/2024).